SOUTHWEST FISHERIES SCIENCE CENTER

NATIONAL MARINE FISHERIES SERVICE - PACIFIC GROVE LABORATORY - 1352 LIGHTHOUSE AVENUE PACIFIC GROVE, CA 93950-2097

MARCH 1999

SEASONAL TO INTERDECADAL VARIABILITY OF THE NORTH PACIFIC CIRCULATION BASED ON THE CLIMATOLOGICAL OBSERVED DATA AND THE PRINCETON OCEAN MODEL

By

Grigory I. Monterey, Lynn deWitt, and Franklin B. Schwing

ADMINISTRATIVE REPORT PG-99-01

SEASONAL TO INTERDECADAL VARIABILITY OF THE NORTH PACIFIC CIRCULATION BASED ON THE CLIMATOLOGICAL OBSERVED DATA AND THE PRINCETON OCEAN MODEL

Grigory I. Monterey, Lynn deWitt, and Franklin B. Schwing

Pacific Fisheries Environmental Laboratory
Southwest Fisheries Science Center
National Marine Fisheries Service, NOAA
Pacific Grove, CA 93950

March 1999

ADMINISTRATIVE REPORT

Contents

Abbreviations

POM - Princeton ocean model
2D, 3D - two-dimensional, three-dimensional
Mode 2 - 2D diagnostic integration of the POM
Mode 4 - 3D diagnostic integration of the POM
DTI - internal mode time step
DTE - external mode time step

SGI - Silicon Graphics Indy workstation
CPU - central processing unit
RAM - random access memory

SST - sea surface temperature
MLD - mixed layer depth

PFEL - Pacific Fisheries Environmental Laboratory
PMEL - Pacific Marine Environmental Laboratory
NODC - National Oceanographic Data Center
NGDC - National Geophysical Data Center
COADS- Comprehensive Ocean-Atmosphere Data Set

SEASONAL TO INTERDECADAL VARIABILITY OF THE NORTH PACIFIC CIRCULATION BASED ON THE CLIMATOLOGICAL OBSERVED DATA AND THE PRINCETON OCEAN MODEL

Grigory I. Monterey, Lynn deWitt, and Franklin B. Schwing

Pacific Fisheries Environmental Laboratory
Southwest Fisheries Science Center
National Marine Fisheries Service, NOAA
Pacific Grove, CA 93950

Abstract

The monthly mean surface wind stress fields for two decades, 1966-1975 and 1977-1986, the climatological monthly mean subsurface temperature and salinity fields, and the bottom topography, all with 1° by 1° horizontal resolution were used as the forcing fields for a North Pacific configuration of the Princeton Ocean Model (POM) to simulate the monthly mean transports for the two decades indicated above. Visualization of the model output illustrates development of numerical instabilities in the case of realistic bottom topography, as well as the results of a number of numerical experiments carried out with different degrees of idealization of the bottom topography. The numerical instabilities originate in limited areas over the steep continental slopes but affect only the baroclinic component of transport. The remaining barotropic plus Ekman components of transport are numerically stable and reproduce the large-scale features of the North Pacific circulation. The monthly mean maps of the forcing fields and of the POM simulated barotropic plus Ekman components of transport for two decades, as well as their differences between the decades, were produced to visualize and animate the seasonal to interdecadal variability of these fields. The animation is available on videotape. Examples of the monthly mean fields indicated above are included in this report. Visualization of the forcing fields and the model simulated transport shows that: the eastern boundary currents are an integral part of the basin-scale circulation; the winter climatological circulation is generally stronger and has a different spatial pattern compared to the summer circulation; during the winter and spring of 1977-1986, the circulation was stronger compared to the circulation during the winter and spring of 1966-1975; and the climatic shift of the North Pacific circulation between the two decades is mainly due to the climatic shift of the surface wind stress.

1. Introduction

This report summarizes some intermediate results as well as a number of unresolved problems encountered in an attempt to develop an ocean modeling system for the simulation, visualization, and retrospective analysis of the seasonal to interdecadal variability of the physical environment of the North Pacific Ocean. This modeling system is intended to produce the monthly mean quantities for the individual years, such as subsurface temperature and salinity, and the horizontal and vertical components of the large-scale circulation, as well as a number of derived quantities, such as the mixed layer depth, the thermocline depth, the vertical thermohaline stratification, and the horizontal and vertical transports of heat, salt, and nutrients. These quantities are thought to be relevant to the decadal-scale variability of biological productivity in the Northeast Pacific.

Decadal fluctuations in biological productivity in the Northeast Pacific and their correlation with the decadal changes in the physical environment were recognized first for the California Current System (Chelton et al., 1982) and later for the area adjacent to the Alaska Current (Brodeur and Ware, 1992). Systematic evidence of a coherent large-scale shift between 1966-1975 and 1977-1986 in wind speed, atmospheric pressure, and SST in the North Pacific was presented by Parrish (1997) based on the surface observations. Recent reviews of the Northeast Pacific ecosystem response to physical regime shifts on the decadal time scale can be found in McGowan et al. (1998), and Holloway and Müller (1998).

The ocean modeling system indicated above is based on a surface data base (Comprehensive Ocean-Atmosphere Data Set, see, e.g., COADS home page: http://www.cdc.noaa.gov/~coads/) and a subsurface data base (World Ocean Data Base, see Levitus et al., 1998), the data retrieval system developed at PFEL (Mendelssohn and deWitt, 1998), the North Pacific configuration of the Princeton Ocean Model that is being developed at PFEL (Monterey and deWitt, 1998), and the graphical application language, Ferret, developed at PMEL (Hankin et al., 1998, see Ferret web site: http://ferret.wrc.noaa.gov/Ferret). The system is designed for multiple runs of the POM forced, e.g., by monthly mean forcing fields for two decades, to simulate transports fields for every month of the two decades indicated above, as well as for the visualization and animation of the forcing fields, the model output, and biologically relevant derived quantities, such as mixed layer depth and thermohaline stratification.

2. The North Pacific configuration of the POM

The POM sample code for a closed rectangular flat bottom basin with analytically prescribed forcing (available from Princeton University) was adapted from a supercomputer version to the UNIX based Silicon Graphics workstation available at PFEL and used as a basis for the development of the North Pacific configuration of the POM code.

- Diagnostic and mixed prognostic/diagnostic modes

In the diagnostic mode of the POM, surface and subsurface forcing fields are held fixed in time, and the circulation spins up from rest to an equilibrium with the forcing fields. In the mixed prognostic/diagnostic mode, only the surface forcing fields (wind stress) are held to their initial conditions, whereas the subsurface forcing fields (temperature and salinity) are allowed to adjust along with the velocity field to an equilibrium with the surface forcing fields.

- The North Pacific topography

The North Pacific coastline and bottom topography were specified in spherical coordinates with 1° by 1° horizontal resolution based on the global topography data set ETOPO60 compiled at NGDC. To avoid the numerical instabilities associated with steep continental slopes, different degrees of idealization of the bottom topography were introduced such as a vertical wall along, e.g., the 500 m isobath. A number of the bottom topography configurations used in this project are specified in the figure captions.

- Boundary conditions

As a first step, the southern boundary of the computational domain was artificially closed by a vertical wall. The southern boundary was chosen where the meridional flows are relatively small. It was set along the latitude of 10°N which is south of the subtropical gyre but north of the North Equatorial Current. Thus, the computational domain had no open boundaries and the POM code execution did not require open boundary conditions. On the side walls and the bottom of the basin the standard closed boundary conditions of the POM were used that correspond to no flow and no advective and diffusive heat and salt fluxes across these boundaries (Blumberg and Mellor, 1985).

- Computational grid

The 3D grid for the North Pacific used in this project contained 130 grid points along the longitude, 52 along the latitude and 24 in the vertical. The horizontal boundaries of the computational domain were defined by the latitudes of 10°N and 62°N and by the longitudes of 120°E and 110°W. The horizontal resolution of the grid is 1° by 1°. The vertical resolution is defined by 24 levels in sigma coordinates. Data on 24 curved sigma surfaces were obtained by spline interpolation (see below) of original data specified at 33 standard z-levels (see, e.g., Levitus and Boyer, 1994, p. 75).

- Forcing fields

The forcing fields for the POM included:

- the monthly mean surface wind stress fields for two decades, 1966-1975 and 1977-1986, compiled at PFEL based on the COADS data,
- the climatological monthly mean subsurface temperature and salinity fields from the World Ocean Data Base (Levitus et al., 1998).

The surface forcing fields are specified on a 1° by 1° horizontal grid. The initial subsurface forcing fields were specified on 33 standard levels in z-coordinates with 1° by 1° horizontal resolution.

- Data conversion block

The POM dynamical equations are formulated and coded in the bottom-following sigma coordinates. Conversion of the subsurface forcing fields from the standard levels in z-coordinates to user-specified curved sigma surfaces is based on the spline interpolation routine developed at Princeton University. The data conversion block was incorporated into the main program of the POM. This is particularly efficient in the POM application for the study of seasonal to interdecadal variability when the model is run numerous times with different forcing fields (e.g., monthly mean for two decades). Use of the data conversion block outside of the POM main program would require storage of monthly mean subsurface forcing fields in sigma-coordinates in addition to the original subsurface data in z-coordinates.

- Modular configuration

To deal with the necessity of numerous modifications and recompilations of the POM, original code was split into the main program and about a dozen subroutines which are stored as separate files and are compiled into an executable file using the UNIX 'make' utility. The modular configuration of the POM is stored on the UNIX-based SGI workstation at PFEL. The instruction for the conversion of the POM code into the modular configuration along with the makefile required for the compilation of the modular configuration of the POM on the UNIX-based computers was contributed to the POM web site (http://www.aos.princeton.edu) maintained at Princeton University.

The advantages of the modular configuration are:

- Quick access to the subroutines without scrolling through thousands of lines of the POM code,
- Compact storage of many versions of each subroutine and main program,
- Replacement and recompilation of the subroutines or the main program without recompilation of the rest of the code.

- *RAM requirements*

In the beginning of the project, the available RAM on the SGI workstation at PFEL was 128 MB, which limited implementation of the POM on a basin scale. The RAM upgrade to 256 MB allowed numerical experiments to be carried out on the 130 x 52 x 24 grid covering the North Pacific with 1° by 1° horizontal resolution. Typical POM runs on the 130 x 52 x 24 grid occupied about 70 % of the 256 MB RAM.

An increase of the horizontal resolution from 1° by 1° to (1/4)° by (1/4)°, which would improve the model's stability, would multiply the required RAM by a factor of 16.

- *Time step*

The external mode time step, DTE, and the internal mode time step, DTI, (Mellor, 1996) were selected to minimize the integration time while satisfying the Courant-Friedrich-Levy (CFL) condition, which is a necessary but not sufficient condition for numerical stability. The formulation of the CFL condition for the POM can be found in Blumberg and Mellor (1987). The external mode solves the vertically integrated dynamical equations. The internal mode resolves the vertical structure of the velocity field. The time steps were chosen as follows: DTE=2 minutes, DTI=1 hour, DTI/DTE=30.

- *Model time*

The model time is defined as the internal mode time step, DTI, times the number of the time steps executed. For example, executing the model over 24 time steps with the internal mode time step set to 1 hour represents 1 day of the model time. Unlike the CPU time (see below) the model time does not depend on the grid size and on the computer power.

As discussed in Section 4, the POM was integrated for up to 30 days of model time.

- *CPU time*

Given DTE=2 minutes and DTI=1 hr, the POM integration for 1 day of model time requires 720 external mode time steps and 24 internal mode time steps. On the SGI with 256 MB of RAM, it takes about 2 minutes of CPU time per day of model time in the case of the 2D computation of transport (Mode 2) on the 130 x 52 grid and about 10 minutes of the CPU time per day of model time in the case of the 3D computation of transport (Mode 3) on the 130 x 52 x 24 grid in sigma coordinates.

3. Diagnostic experiments

In the diagnostic mode, the North Atlantic configuration of the POM was reported to approach an equilibrium after 5-7 days of integration (the model time) based on the time behavior of the area-averaged kinetic energy (Ezer and Mellor, 1994). However, it was not explicitly shown that the velocity field itself does not continue to evolve in time after 5-7 days of integration.

- *The topographic limit of applicability*

The POM applicability in its present formulation is known to be limited by the condition $\Delta H/H < \sim 0.4$, where H is the ocean depth and ΔH is the depth difference between adjacent grid points (Ezer and Mellor, 1997). Within the 1^0 by 1^0 degree horizontal resolution this condition is not satisfied in some areas of the upper continental slope of the North Pacific basin. The above condition can be fulfilled by artificially reducing the steepness of the continental slope. The POM implementations with smoothed bottom topography may be of use for a qualitative analysis of the impact of different components of forcing (e.g., wind stress and the subsurface density gradients) on the circulation. However, a quantitative analysis of the North Pacific circulation, such as estimates of transports of California and Alaska currents, require use of the original topography, particularly in the areas of the Northeast Pacific continental slopes where these eastern boundary currents are situated. This limitation of the POM can be addressed by increasing the horizontal resolution in areas over the steep continental slopes.

- *Model instability*

Attempts to integrate the North Pacific configuration of the POM with the realistic bottom topography specified with 1° by 1° horizontal resolution resulted in the model becoming unstable after about one day of integration. Specifically, the simulated velocity field at some locations developed unreasonably large magnitudes that triggered an abnormal end of the POM code execution. As illustrated by Figures 1 and 2, the numerical instability originates in limited areas over a steep continental slope. As illustrated by Figure 1, in the case of the artificial vertical wall imposed along the 200-m isobath, there are two areas of instability after one day of integration, one on the eastern and one on the western sides of the North Pacific basin at about 25°N. As illustrated by Figure 2, a vertical wall imposed along the 500-m isobath eliminates the source of instability on the eastern side of the basin. Thus the instabilities originate over the steepest upper part of the continental slope adjacent to the continental shelf at depths between 200 m and 500 m. Note that if ocean depths at adjacent grid points are, for example, 200 m and 500 m, then the ratio of $\Delta H/H$ is ~ 1 in violation of the POM applicability limit discussed in the previous section.

- Stable cases

In several situations characterized by different degrees of idealization, the model integration was carried out for up to 30 days and produced reasonable results.

Figures 3 (a),(b),(c) show the vertically integrated total transport after 2, 10 and 30 days of the POM integration respectively in the case of the North Pacific basin with a realistic coastline, a flat bottom at 1000-m depth, a vertical wall along the 1000-m isobath and forcing by the climatological annual mean surface wind stress, analytically prescribed subsurface temperature that roughly simulates the 3D thermal structure of the subtropical and the subpolar gyres, and constant salinity.

Figures 4 (a),(b) show the total transport after 15 days of the POM integration in Mode 4 (vertical structure resolved) and in Mode 2 (only vertically integrated equations are involved), respectively, in the case of forcing by the climatological wind stress, the climatological subsurface temperature and salinity, and the same idealized bottom topography as in Fig. 3. Integration in Mode 2 takes about 5 times less CPU time compared to Mode 4. The nearly identical transport patterns of Figures 4 (a) and 4 (b) illustrate that in this case Mode 2 is a good approximation of Mode 4.

The POM simulated total transport shown in Figures 3 and 4 contains the main features of the North Pacific large-scale circulation, such as the Kuroshio and Oyashio on the western side of the basin and the California and Alaska currents on the eastern side of the basin. However, the quantitative characteristics of the simulated velocity field, such as the relative strengths of the California and Alaska currents, distance of the California Current from the shore, and strength of the northward nearshore countercurrent in the California Current region are significantly altered by the idealization of the North Pacific bottom topography.

Figures 5 (a),(b),(c) show the total transport after 1, 2 and 15 days, respectively, of the POM integration in Mode 2 in the case of a vertical wall along the 1000-m isobath, realistic bottom topography below the 1000-m depth level, and forcing by the climatological annual mean surface wind stress, the analytically prescribed subsurface temperature, the same as in Figure 3, and constant salinity. In this case (Fig. 5), the circulation contains more sub-basin scale detail compared to the case with the flat bottom (Fig. 3).

As explained above, in the case of realistic bottom topography, realistic subsurface forcing fields and 1° by 1° horizontal resolution, the POM could not be integrated long enough for the simulated velocity field to approach an equilibrium with the forcing fields due to numerical instabilities in limited areas situated over the steep bottom slope.

In an attempt to avoid the numerical instability described above, the velocity field was decomposed into the baroclinic, barotropic, and Ekman components driven by the horizontal components of the subsurface density gradient, the slope of the sea surface, and the surface wind stress, respectively (see, e.g., Isayev and Levitus, 1995). Analysis of the results of a number of numerical experiments shows that the numerical instability is limited to the baroclinic component.

Numerical experiments were carried out with the baroclinic component of the velocity field

artificially eliminated (multiplied by zero at every time step). In this case the POM integration with 1° by 1° horizontal resolution could proceed, and produced the remaining barotropic and Ekman components of the velocity field and the corresponding vertically integrated transport field that depend on the wind stress and the slopes of sea level and bottom depth, but do not depend on the horizontal components of the subsurface density gradient. In this case the model was integrated for up to 30 days. This is illustrated by Figures 6 (a),(b),(c) that show the barotropic plus the Ekman components of transport after 5, 10, and 30 days of integration, respectively. As illustrated by Figure 6(a), 5 days of the POM integration results in a somewhat realistic signal. However, further integration of the POM generates noise that increases with time. After 30 days of integration it overrides the signal in some areas, mostly on the western side of the basin (Fig. 6(c)).

4. Seasonal to interdecadal variability

To approximately simulate, e.g., the velocity field for January of 1966-1975, the POM was integrated in diagnostic mode for 5 days forced by the wind stress for January of 1966-1975 and January climatological subsurface temperature and salinity fields, etc. The subsurface climatology was used instead of decadal fields due to considerable gaps in subsurface observations, particularly for salinity. The same procedure was repeated for each month of 1966-1975 and 1977-1986 to compute the monthly mean transports for the two decades as well as their differences between the decades. Due to numerical instability of the baroclinic component only the Ekman and barotropic components were computed. The examples of the monthly mean fields used for the analysis of the seasonal to interdecadal variability as well as for creating an animation of the seasonal cycle of the above fields are shown in the Appendix.

The observed and the POM simulated fields indicated above display the following noticeable features of the North Pacific circulation and the thermohaline structure:

- the eastern boundary currents are an integral part of the regional-scale circulation,
- during winter the Subtropical Gyre and the eastern boundary currents are generally stronger than during summer,
- during the winter and spring of 1977-1986 the subtropical and the subpolar gyres were generally stronger than during the winter and spring of 1966-1975 (see last four figures in the Appendix, not numbered).

5. Discussion and summary

The interdecadal variability of ocean circulation and thermohaline structure is easier to detect when approached on the seasonal or monthly mean rather than annual mean basis. In particular, the differences between 1966-1975 and 1977-1986 of the physical parameters such as surface wind stress, and Ekman and barotropic transport are noticeable during late winter and spring and are not well expressed during the rest of the year.

Subsurface observations of temperature and particularly salinity are much more sparse compared to the surface observations. Whereas the 1° by 1° fields of the surface wind stress and SST for every month of the individual years were produced based on the COADS observations (DaSilva, et al., 1994), sparseness of the subsurface observations does not allow to compile the 1° by 1° monthly mean temperature and salinity fields for individual years.

For the purpose of a retrospective analysis of the decadal variability of the ocean circulation and thermohaline structure, a model design is necessary that could start with the climatological monthly mean subsurface temperature and salinity fields and adjust them to the corresponding monthly mean fields for the individual years based on the model dynamics and the available surface forcing fields for the individual years.

In principle, the POM has the capability to perform such an adjustment. This could be done in two stages. The first stage is the POM integration in the diagnostic mode with the surface and subsurface forcing fields held fixed in time to spin up the velocity field from rest to equilibrium with the forcing fields. At this stage the available subsurface climatology can be used along with the surface forcing fields for the individual years. The second stage is the POM integration in a combination of the diagnostic and the prognostic modes. In this stage only the surface forcing fields are held fixed in time whereas the subsurface temperature and salinity fields are allowed to evolve from their climatological monthly mean states to the monthly mean states for the individual years.

Intermediate results presented in this report are intended to illustrate the diagnostic stage of the POM application to the North Pacific. Even in this stage a problem of numerical instability of the baroclinic component of circulation associated with steep continental slopes and insufficient horizontal resolution remains to be resolved. This problem can be addressed by increasing the resolution in areas of steep continental slopes, which would require access to a supercomputer and/or an implementation of a variable horizontal resolution.

On the other hand, the POM simulated barotropic and Ekman components of transport are numerically stable and contain main features of the North Pacific large-scale circulation, such as the North Pacific Current, California Current and Alaska Current as well as their seasonal to interdecadal variability.

Acknowledgements

We thank George Mellor, William O'Connor, Tal Ezer, and Igor Shulman for valuable advice on the Princeton Ocean Model, Steven Hankin for support on the graphical application language Ferret, Sydney Levitus and Timothy Boyer for advice on the World Ocean Atlas data base, Roy Mendelssohn for advice on the data retrieval system developed at PFEL, Richard Parrish and Tom Murphree for stimulating comments on climatic variability in the North Pacific, Arthur Stroud for the computer system administration, Steven Cummings for technical assistance. PFEL Director George Boehlert supported this project by general advice, encouragement and by making available the PFEL computer resources. This work is funded in part by NSF and NOAA COP as part of the US GLOBEC Northeast Pacific (NEP) Program.

References

Blumberg, A.F., and G.L. Mellor (1987) A description of a three-dimensional coastal ocean circulation model, In *Three-dimensional Coastal Ocean Models, Coastal Estuarine Sci.*, Vol. 4, edited by N.Heaps., pp. 1-16, AGU, Washington, D.C.

Brodeur, R.D. and D.M. Ware (1992) Long-term variability in zooplankton biomass in the subarctic Pacific Ocean. *Fish. Oceanogr.*, **1**: 32-38.

Chelton, D.B., P.A. Bernal and J.A. McGowan (1982) Large-scale interannual physical and biological interaction in the California Current. *J. Mar. Res.*, **40**:1095-1125.

DaSilva, A.M., C.C. Young, and S. Levitus (1994) Atlas of surface marine data. *NESDIS NOAA,* Vol. 1, Washington, D.C., 83 pp.

Ezer, T., and G.L. Mellor (1994) Diagnostic and prognostic calculations of the North Atlantic circulation and sea level using a sigma coordinate ocean model. *J. Geophys. Res.*, **99**, No C7, 14,159-14,171.

Ezer, T., and G.L. Mellor (1997) Simulations of the Atlantic Ocean with a free surface sigma coordinate ocean model. *J. Geophys. Res.*, **102**, No C7, pp. 15647-15657.

Holloway, G. and P. Müller (1998) Workshop considers biotic impacts of extratropical climate variability in the Pacific. *Eos, Trans. Am. Geophys.Union,* **79**, No 34: 407.

Isayev, G., and S. Levitus (1995) A diagnosis of the North Atlantic horizontal and vertical circulation with error estimates. *J. Geophys. Res.*, **100**, No C4., pp. 6795-6815.

Levitus, S., T.P. Boyer, M.E. Conkright, T. O'Brien, J. Antonov, C. Stephens, L. Stathoplos, D. Johnson, R. Gelfeld (1998) *NOAA Atlas NESDIS 18,WORLD OCEAN DATABASE 1998*: Vol. 1: Introduction, U.S. Gov. Printing Office, Wash., D.C., 346 pp.

Levitus, S., and T.P. Boyer (1994) *World Ocean Atlas, NOAA NESDIS 4,* Temperature, 117 pp., Washington, D.C.

Levitus, S., R.Burgett, and T.P.Boyer (1994) *World Ocean Atlas, NOAA NESDIS 3*, Salinity, 99 pp., Washington, D.C.

McGowan, J.A., D. Cayan, and L.M. Dorman (1998) Climate-Ocean variability and ecosystem response in the Northeast Pacific. *Science*, **281**: 210-217.

Mellor, G.L. (1996) Users guide for a three-dimensional, primitive equation, numerical ocean model, 39 pp., Princeton University.

Mendelssohn, R., and L. DeWitt (1998) Accessing and visualizing archived and near real-time data sets for monitoring oceanographic change. *Abstracts of the 45-th Annual Eastern Pacific Ocean Conference (EPOC)*, p. 30, Mt. Hood, Oregon.

Monterey, G., and L. DeWitt (1998) Seasonal cycle of the North Pacific circulation based on the climatological data and the Princeton Ocean Model. Proceedings of the Princeton Ocean Model workshop, Miami, p. 32.

Monterey, G., and L. DeWitt (1998) Seasonal to Interdecadal variability of the North Pacific circulation based on the climatological data and the Princeton Ocean Model. Ocean Sciences Meeting, San Diego. EOS, **79**, No 1, p.OS73.

Parrish, R.H. (1997) Regime-scale fluctuations in the circulation of the North Pacific. *Proceedings of the workshop: Estuarine and Ocean Survival of Northeastern Pacific Salmon. NOAA Tech. Memorandum NMFS-NWFSC*-29, pp. 95-103.

List of Figures

Fig. 1. The POM simulated total transport after 1 day of integration for the case of a vertical wall along the 200 m isobath, realistic bottom topography below the 200 m level, and forcing by the climatological annual mean surface wind stress and the analytically prescribed subsurface temperature and salinity.

Fig. 2. The POM simulated total transport after 1 day of integration for the case of a vertical wall along the 500 m isobath, realistic bottom topography below the 500 m level, and forcing by the climatological annual mean surface wind stress and the subsurface temperature and salinity fields.

Fig. 3 (a), (b), (c). The POM simulated total transport after 2, 10 and 30 days of integration for the case of a vertical wall along the 1000 m isobath, a flat bottom at the 1000 m level, and forcing by the climatological annual mean surface wind stress and the analytically prescribed subsurface temperature and salinity.

Fig. 4 (a), (b). The total transport after 15 days of the POM integration in Mode 4 (vertical structure resolved) and Mode 2 (only vertically integrated equations are solved) for the case of forcing by the climatological annual mean surface wind stress and the subsurface temperature and salinity. The bottom topography is the same as in Fig. 3.

Fig. 5 (a), (b), (c). The POM simulated total transport after 1, 2 and 15 days of integration for the case of the vertical wall along the 1000 m isobath, realistic bottom topography below the 1000 m level, and forcing by the climatological annual mean surface wind stress and the analytically prescribed subsurface temperature and salinity.

Fig. 6 (a), (b), (c). The POM simulated barotropic plus Ekman components of transport after 5, 10 and 30 days of integration for the case of the realistic bottom topography and forcing by the climatological January mean surface wind stress and the subsurface temperature and salinity.

Appendix. Examples of figures that were used to create the animation of seasonal cycle. These figures show the bottom topography; the forcing fields: the observed climatological subsurface temperature and salinity, and surface wind stress; and the POM simulated barotropic plus Ekman component of transport. All of the above fields except the bottom topography are for January and July of two decades, 1966-1975 and 1977-1986.

Fig. 1

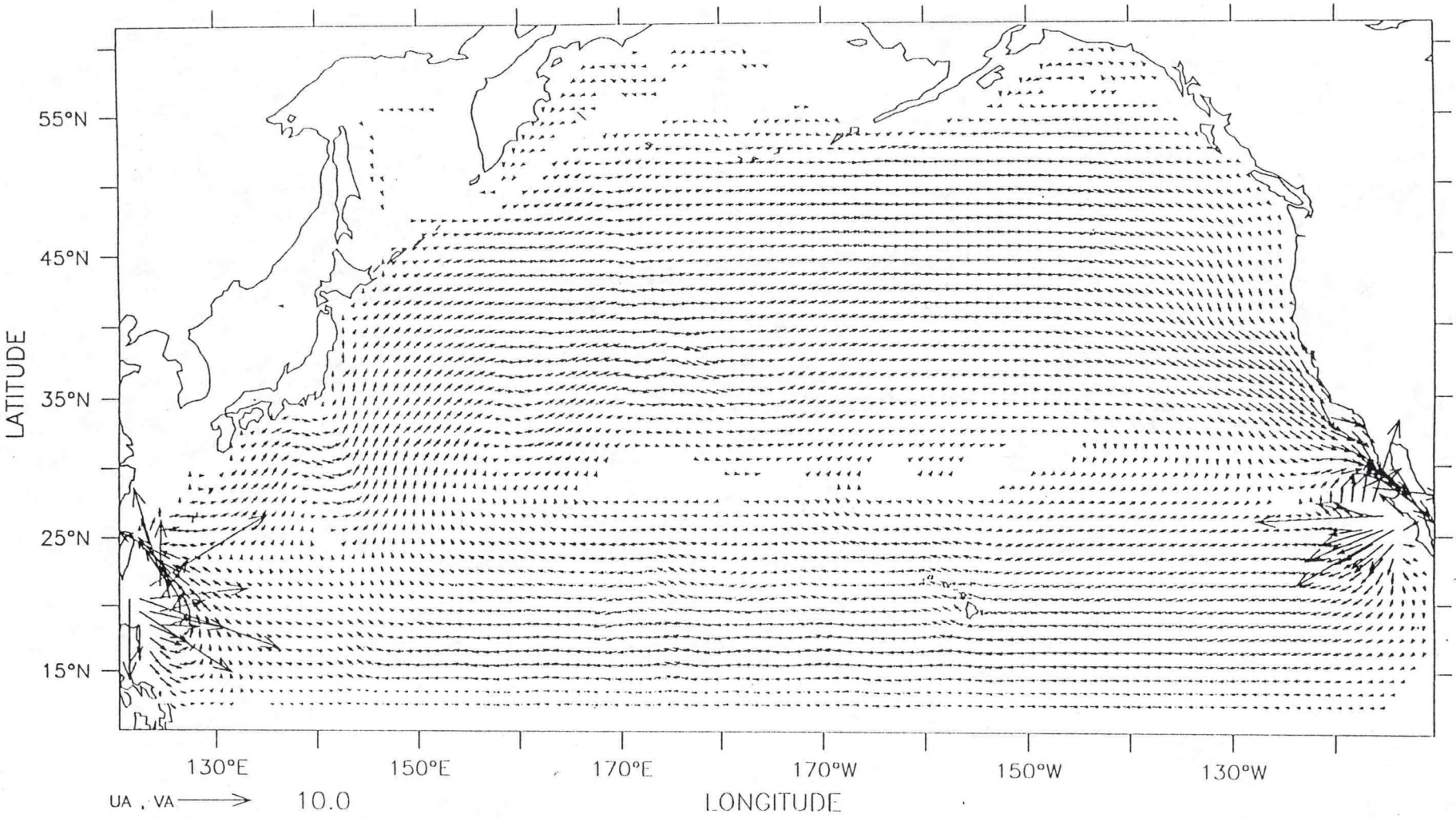

Total transport (Sv)

Fig. 2

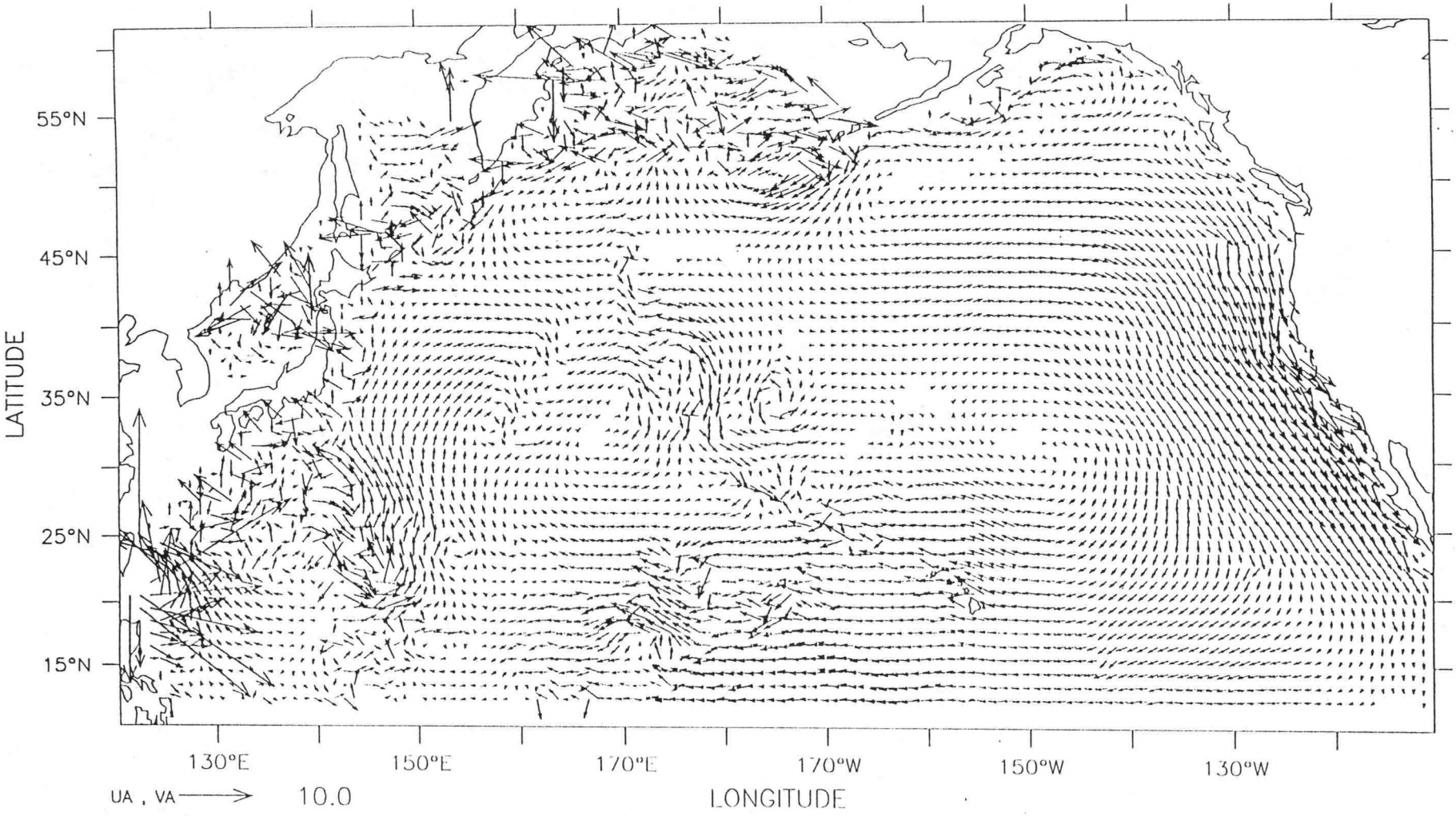

Total transport (Sv)

Fig. 3(a)

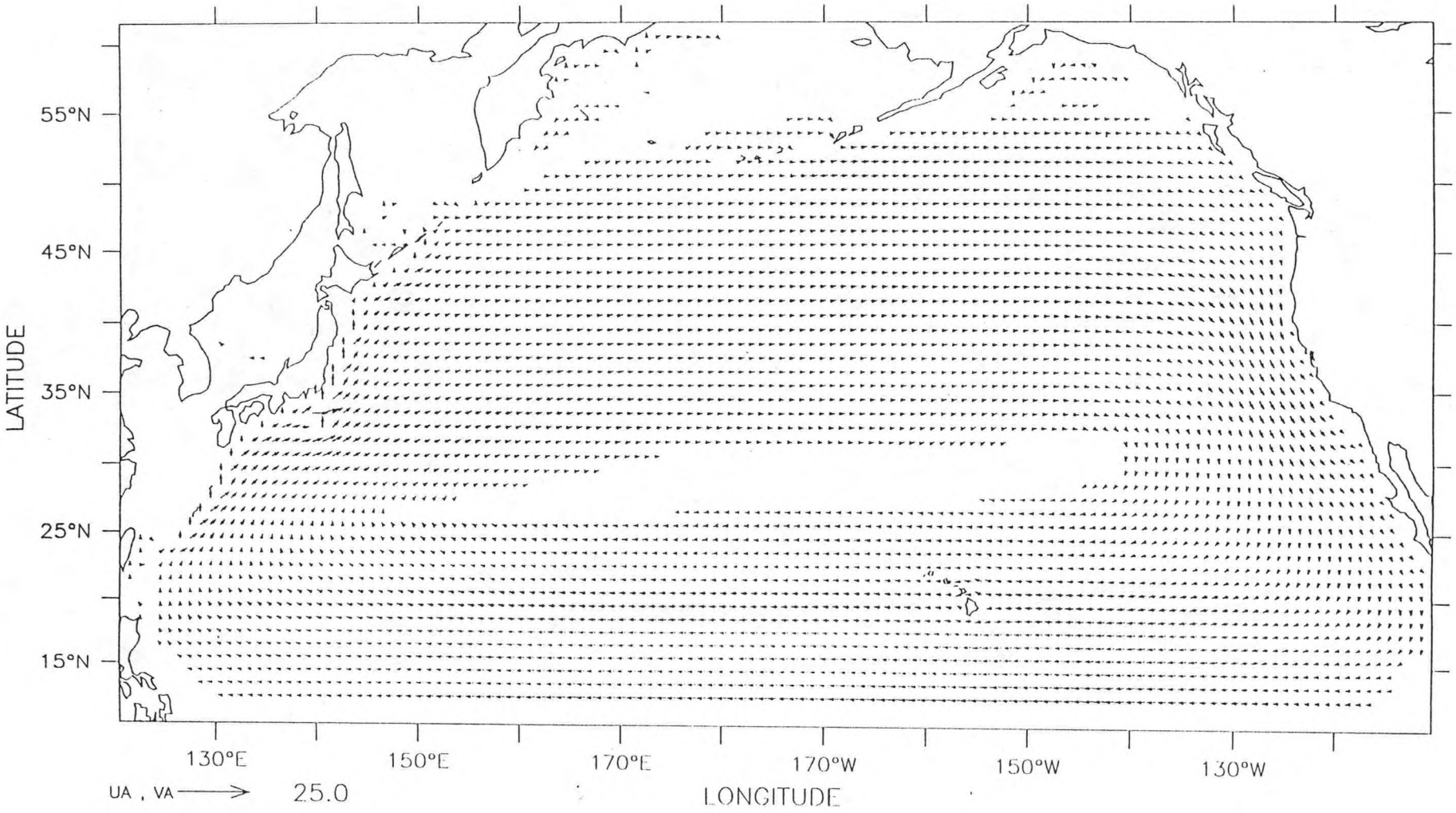

Total transport (Sv)

Fig. 3(b)

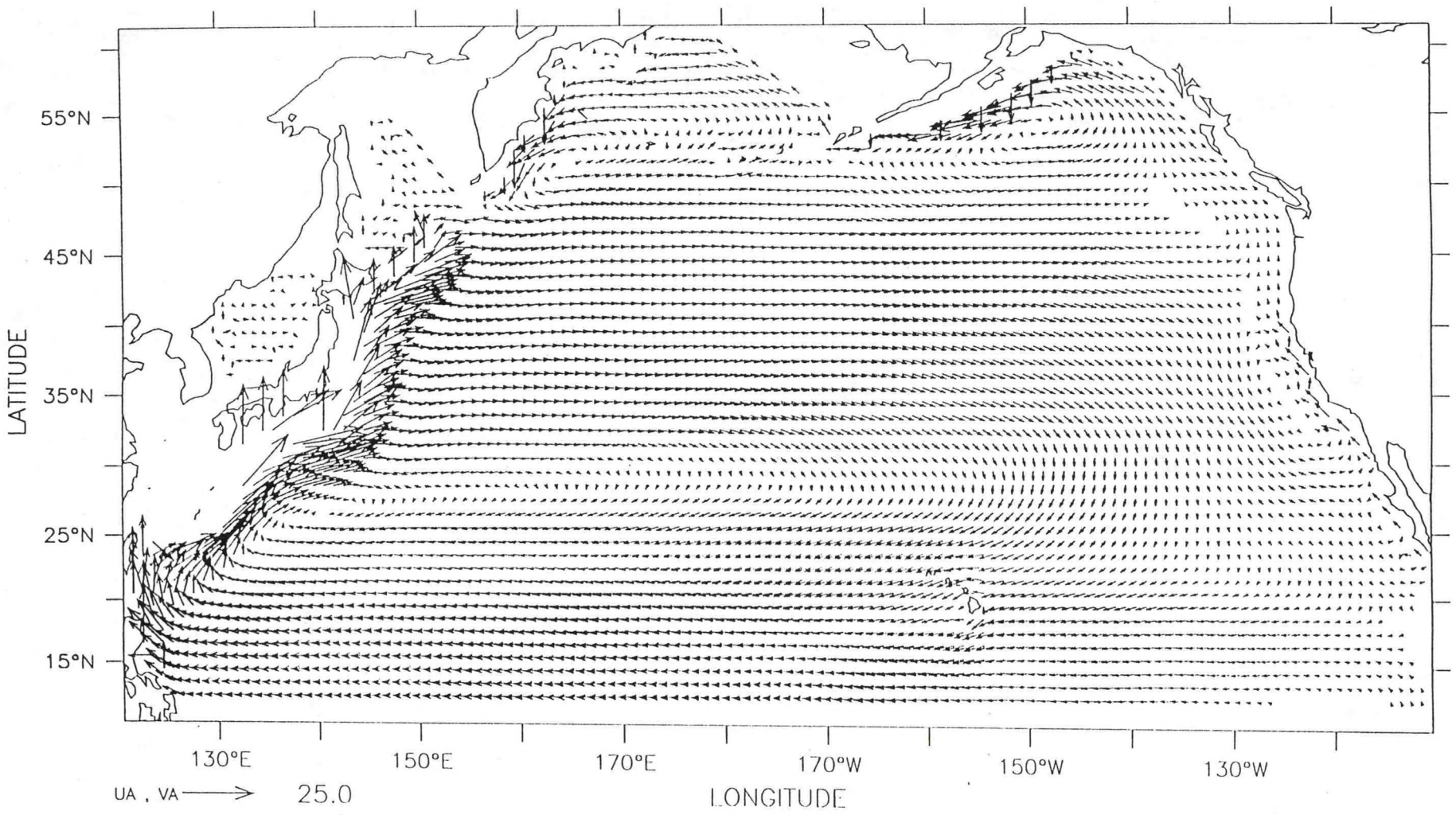

Total transport (Sv)

Fig. 3(c)

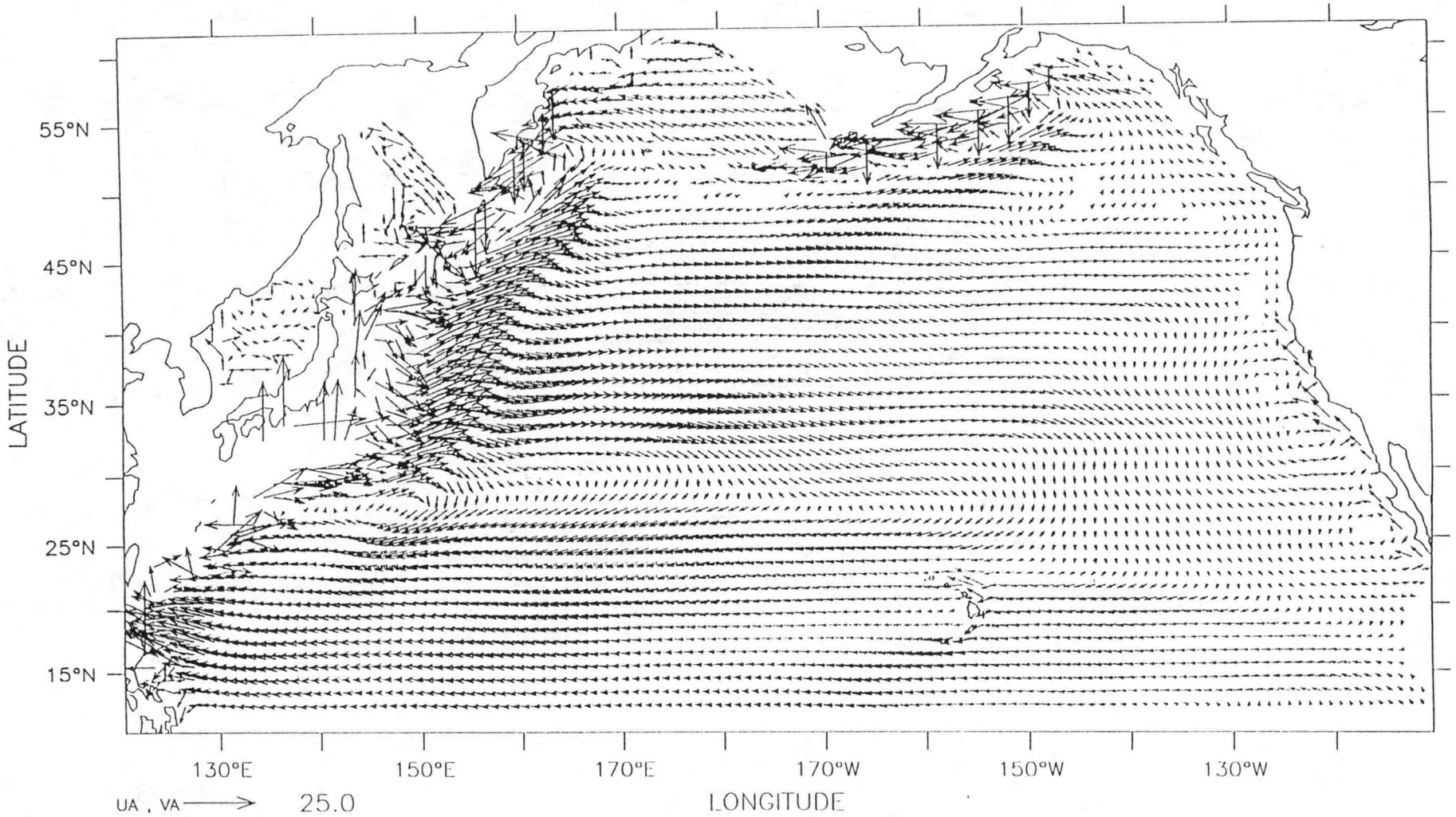

Total transport (Sv)

Fig. 4(a)

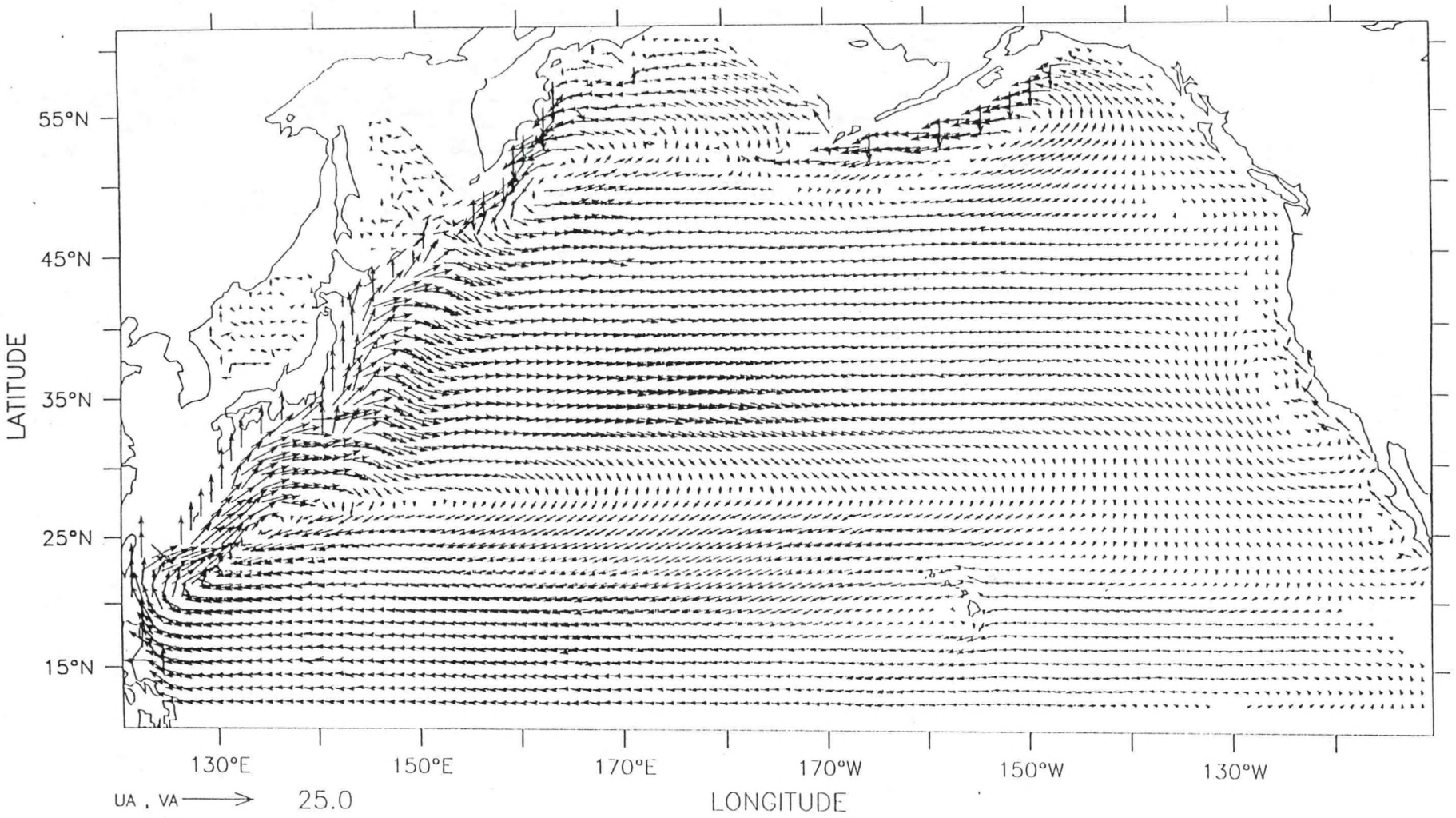

Total transport (Sv)

Fig. 4(b)

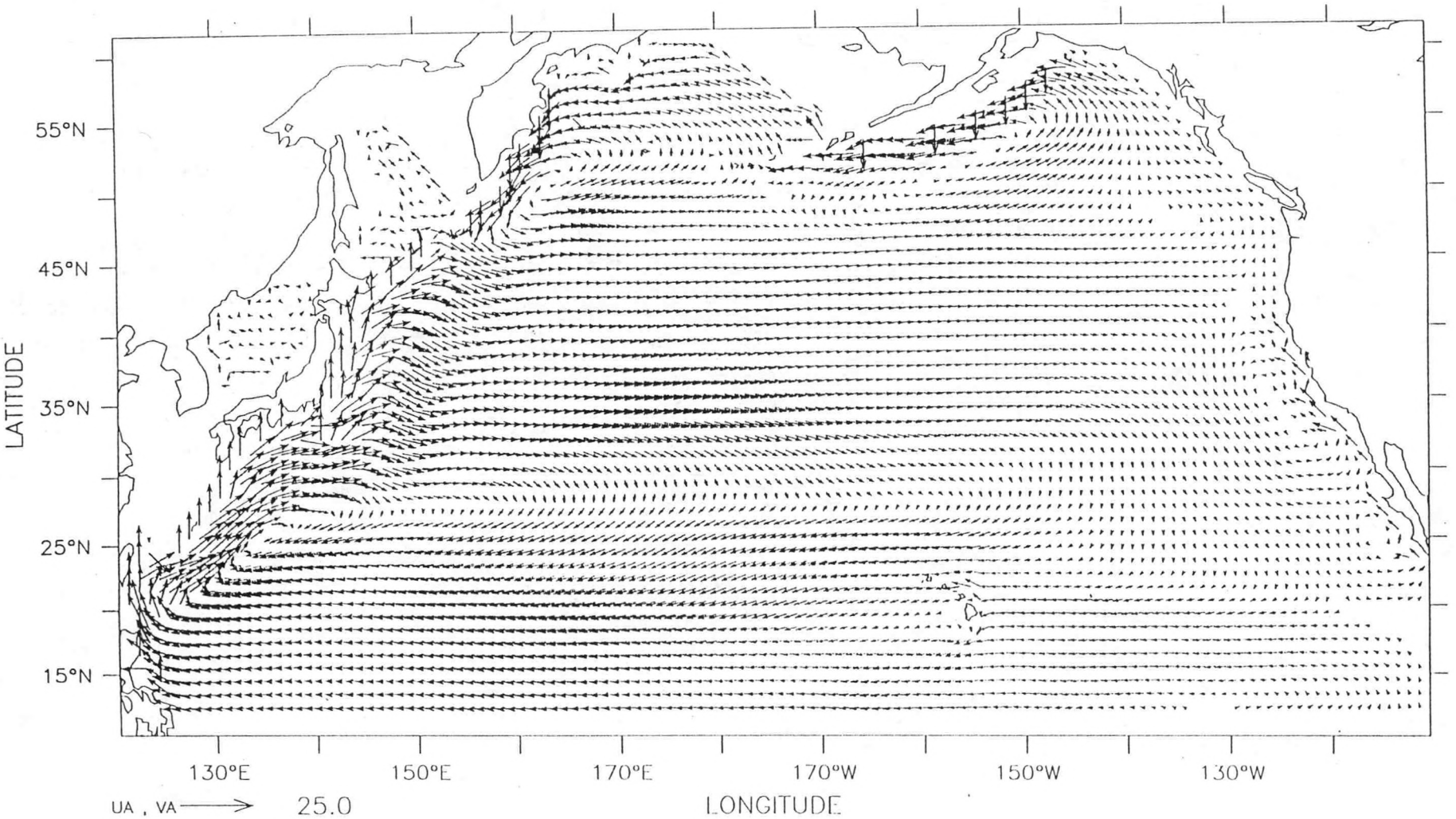

Total transport (Sv)

Fig. 5(a)

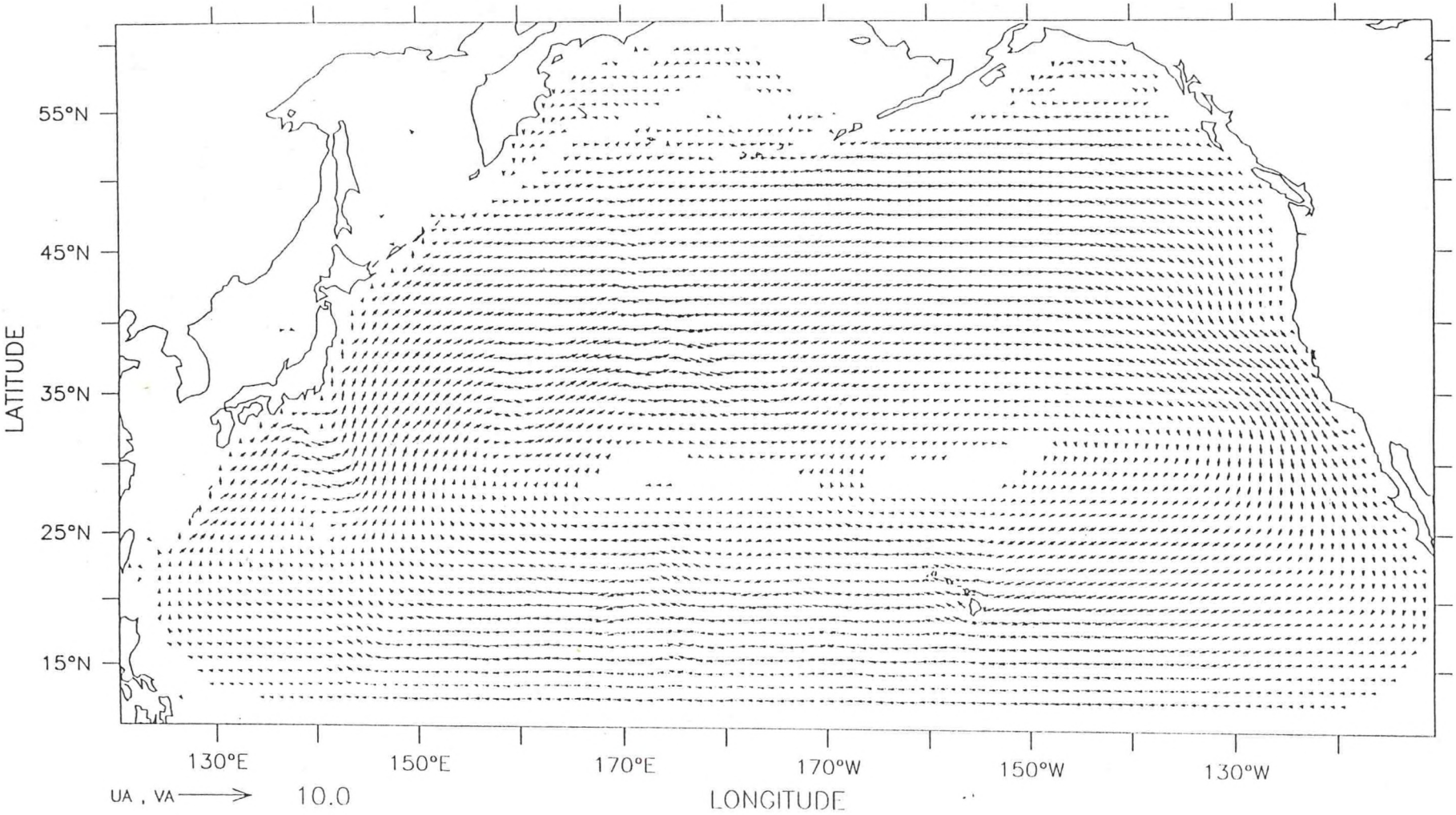

Total transport (Sv)

Fig. 5(b)

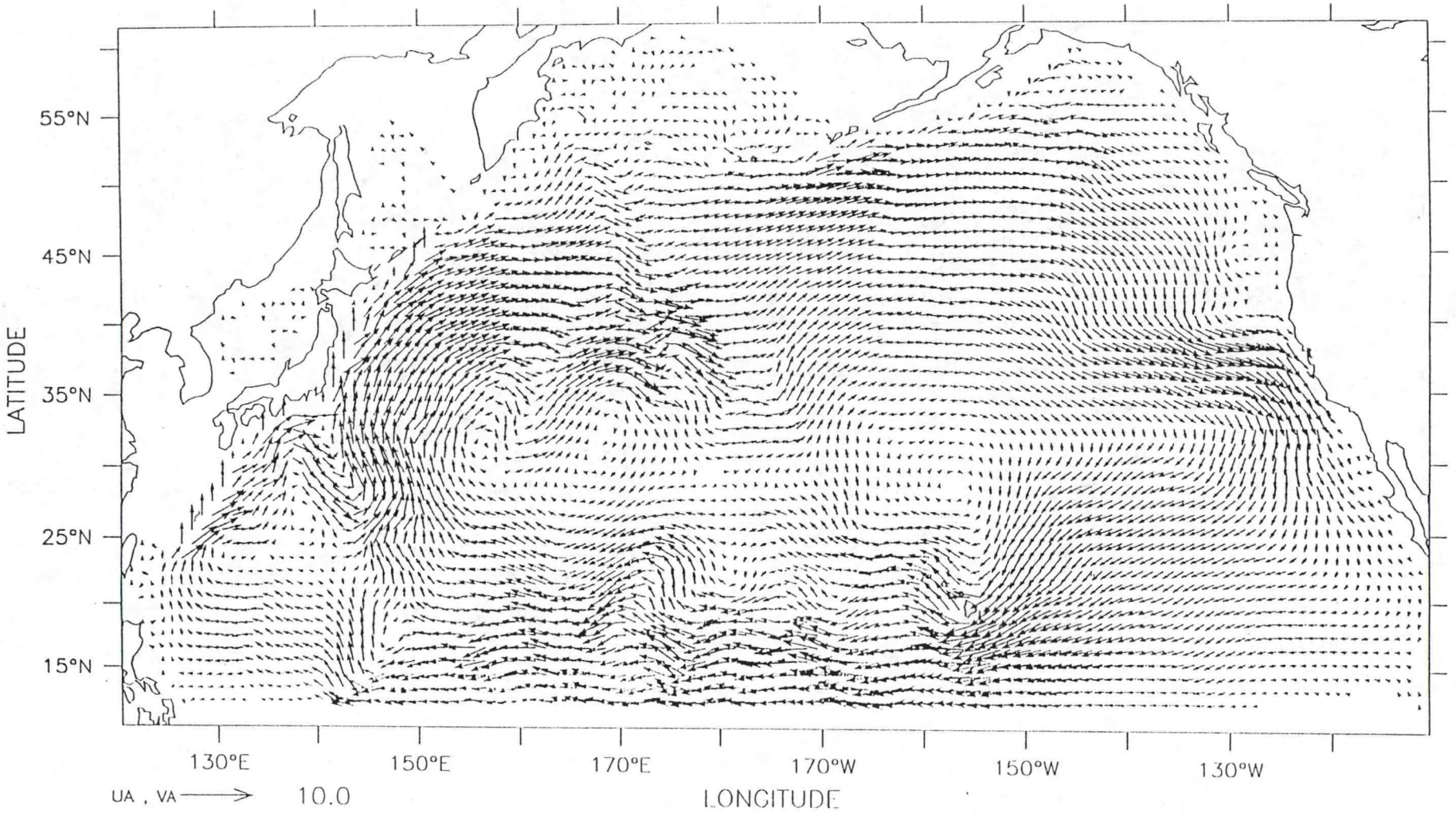

Total transport (Sv)

Fig. 5(c)

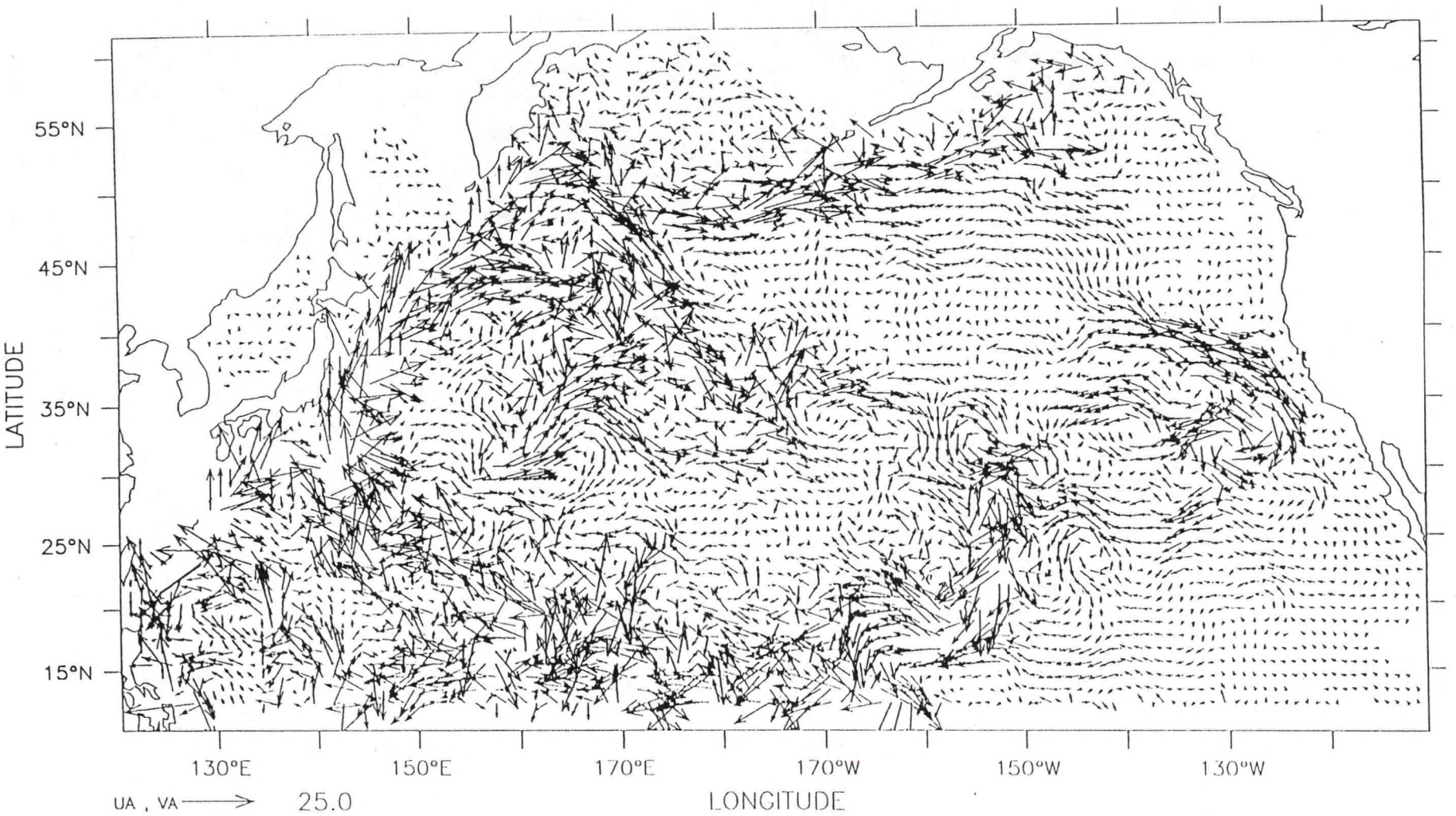

Total transport (Sv)

Fig. 6(a)

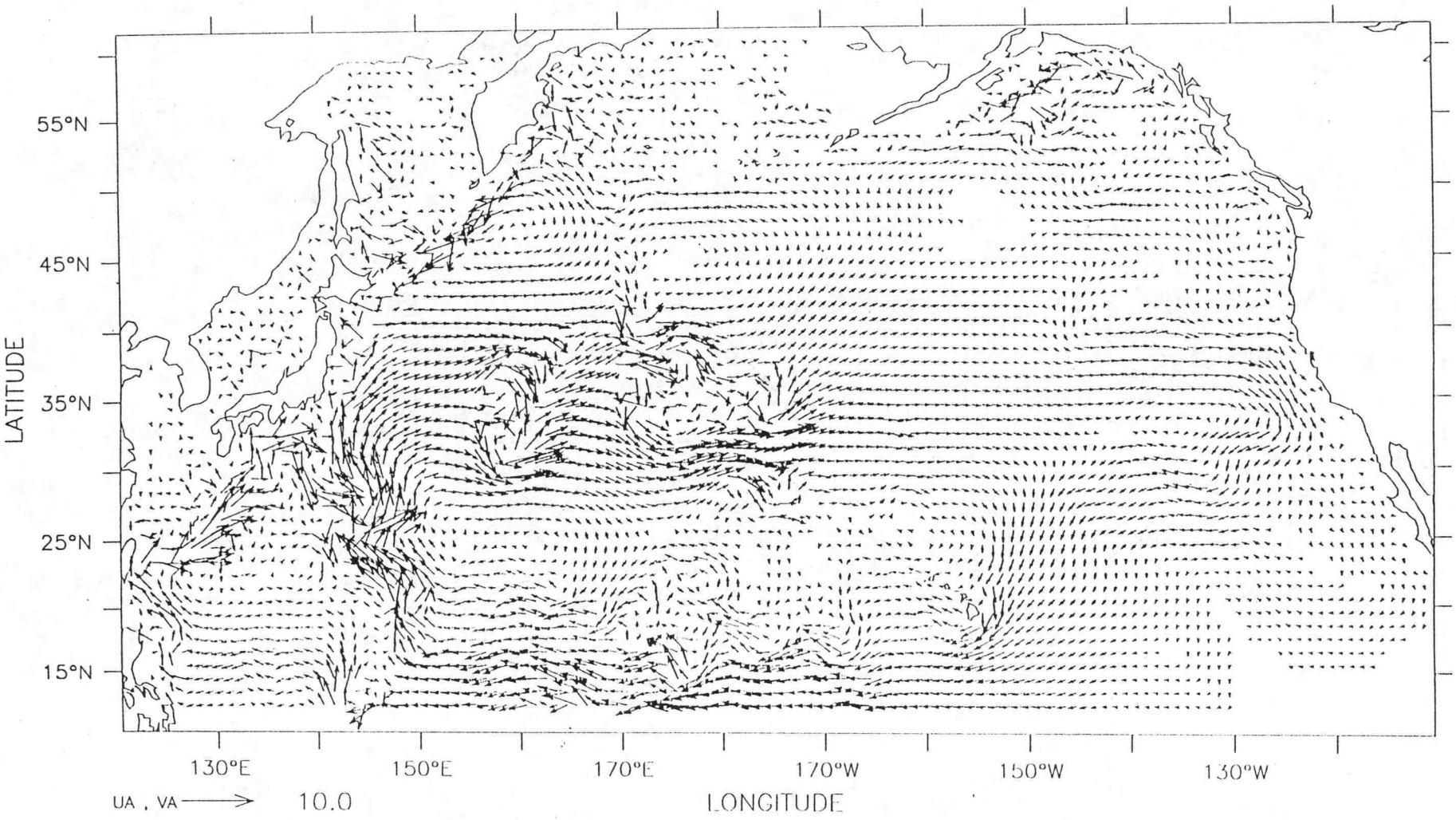

Barotropic plus Ekman transport (Sv)

Fig. 6(b)

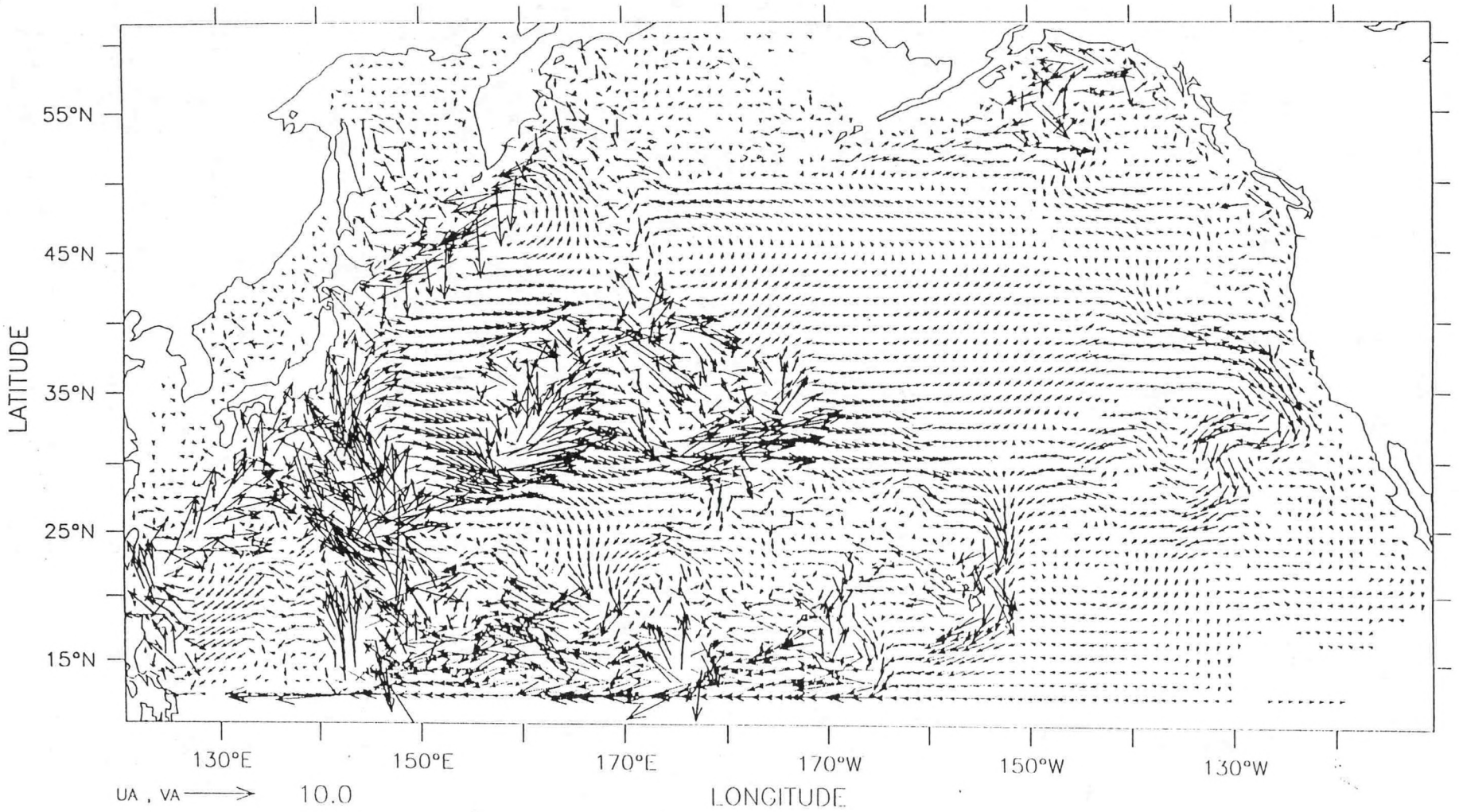

January mean transport (Sv)

Fig. 6(c)

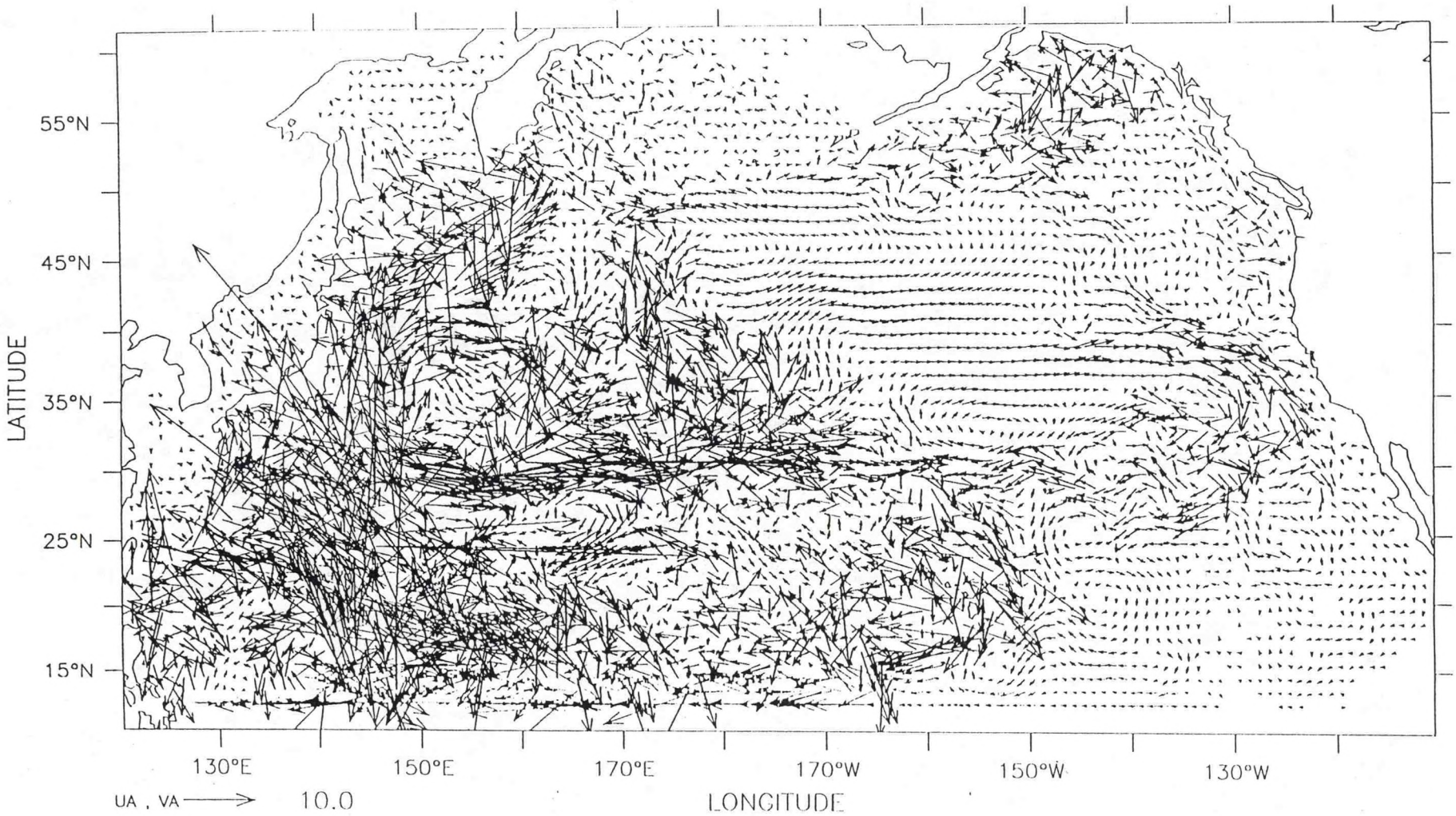

January mean transport (Sv)

Appendix

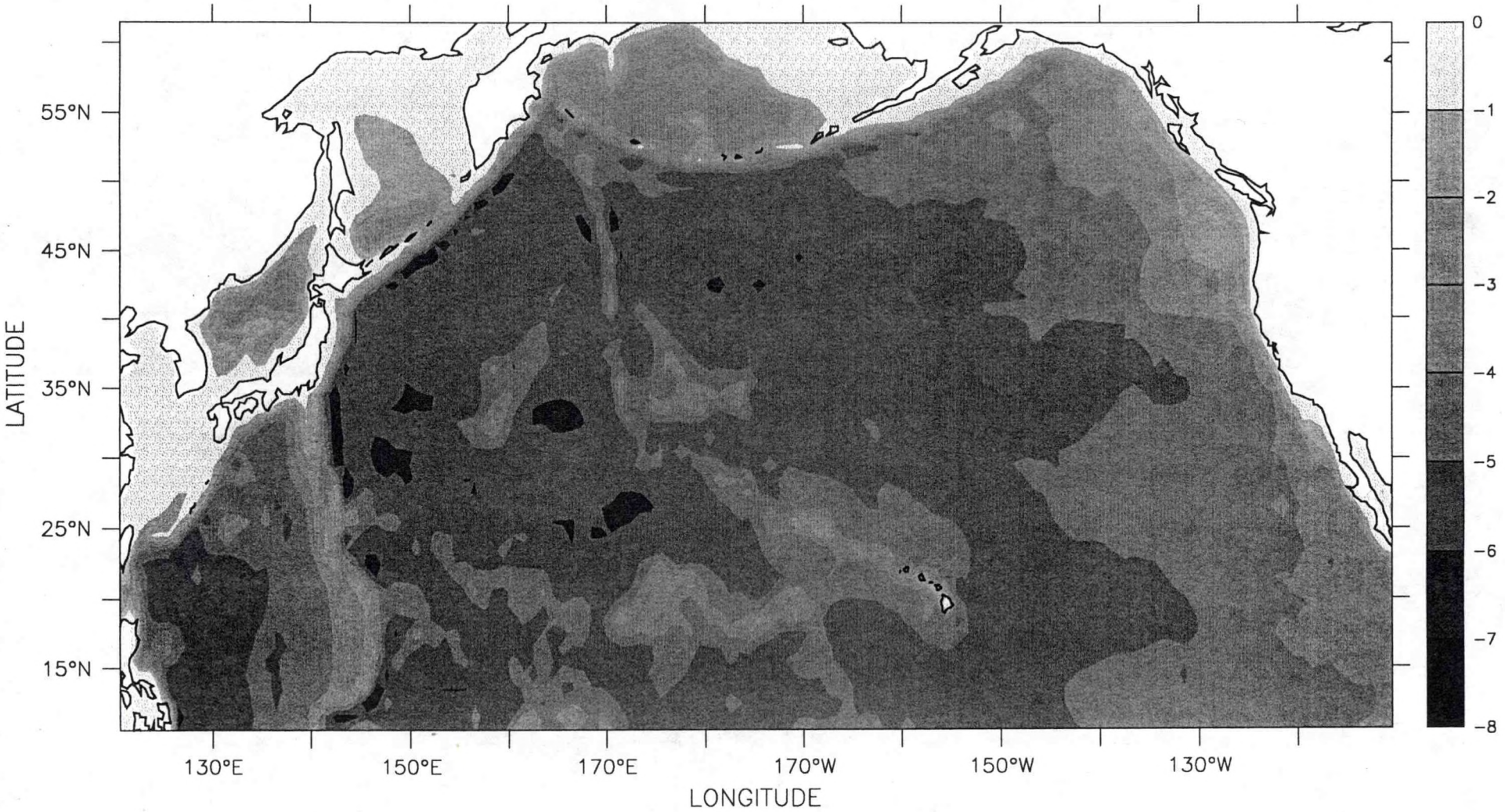

Bottom Topography

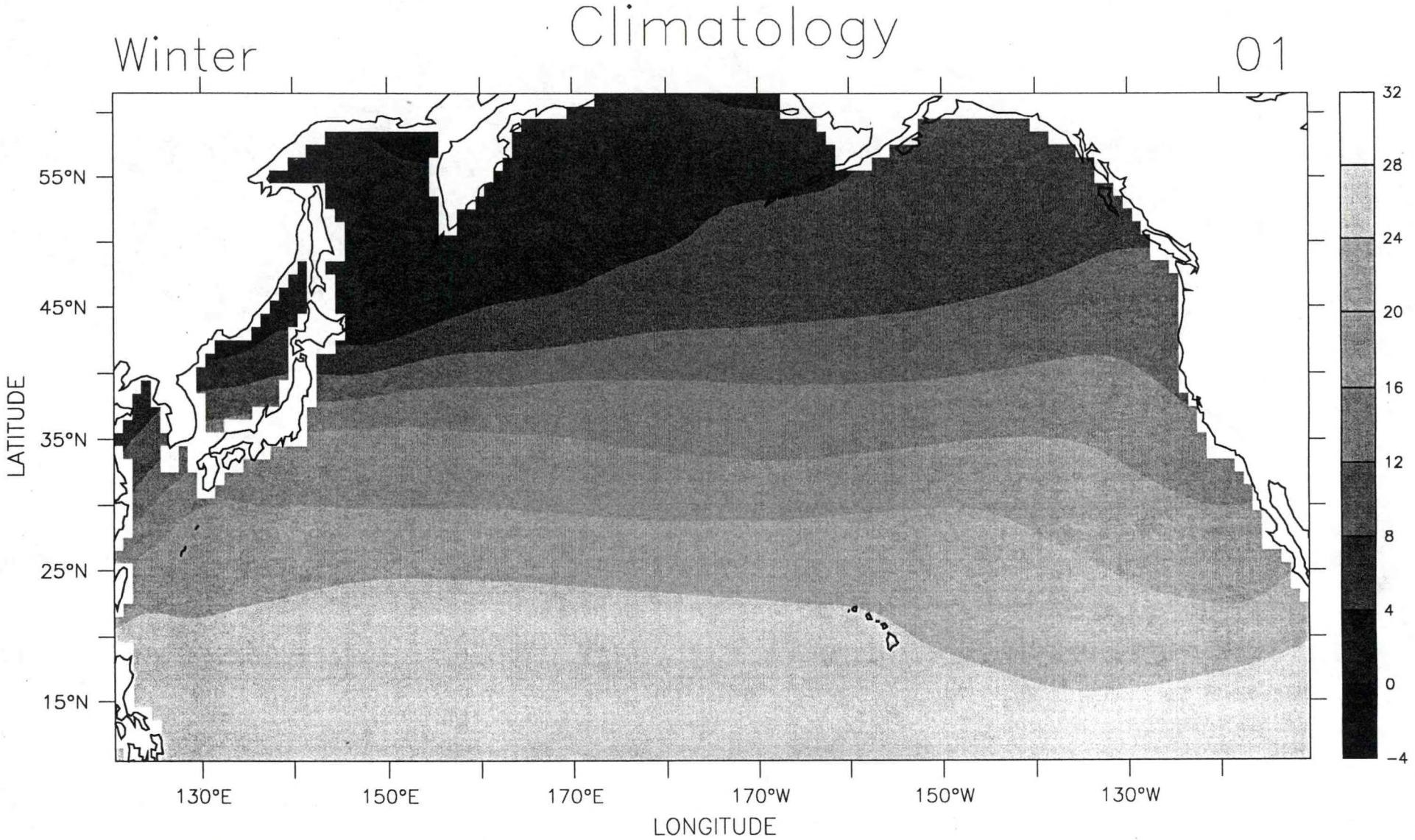

Surface Temperature (C)

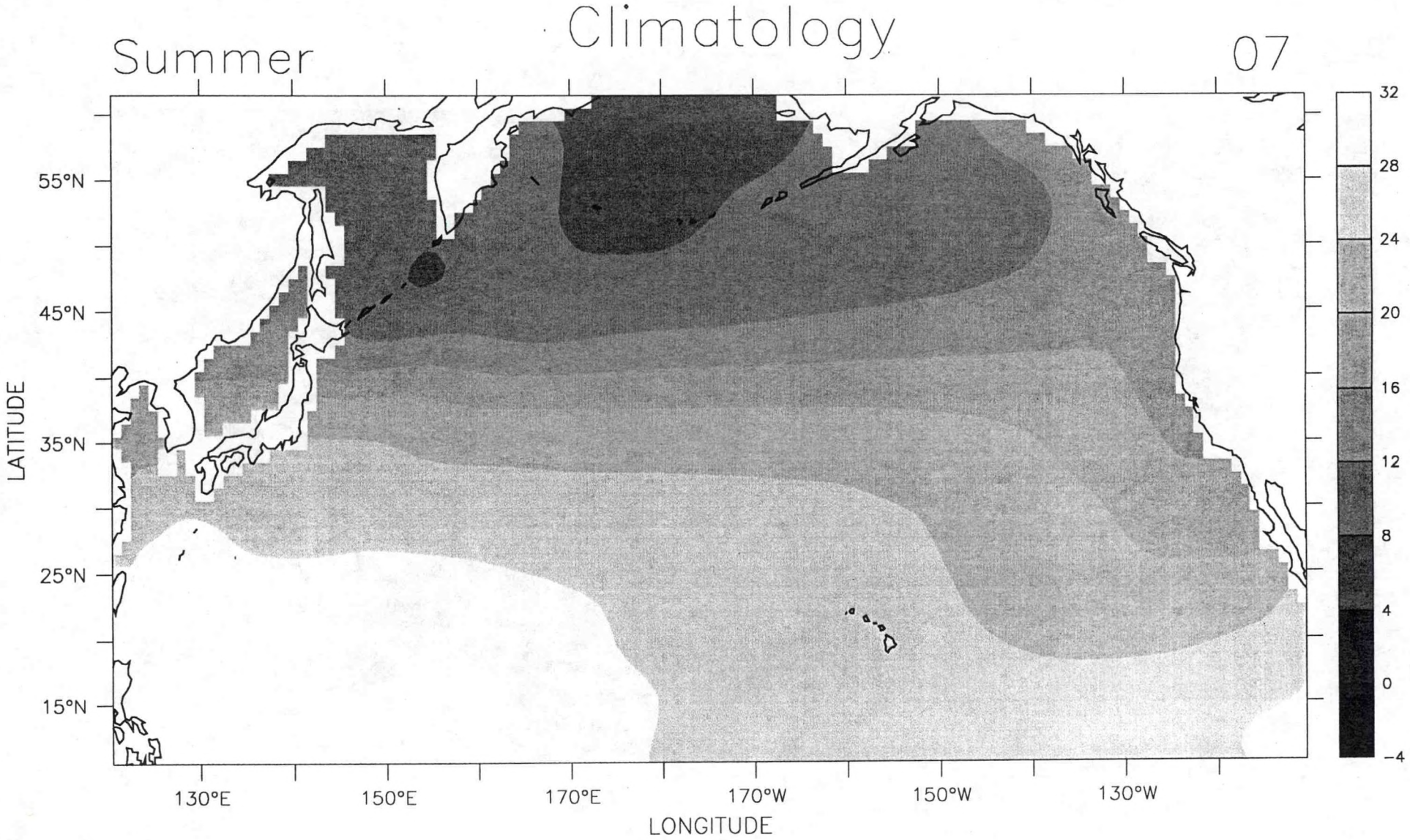

Surface Temperature (C)

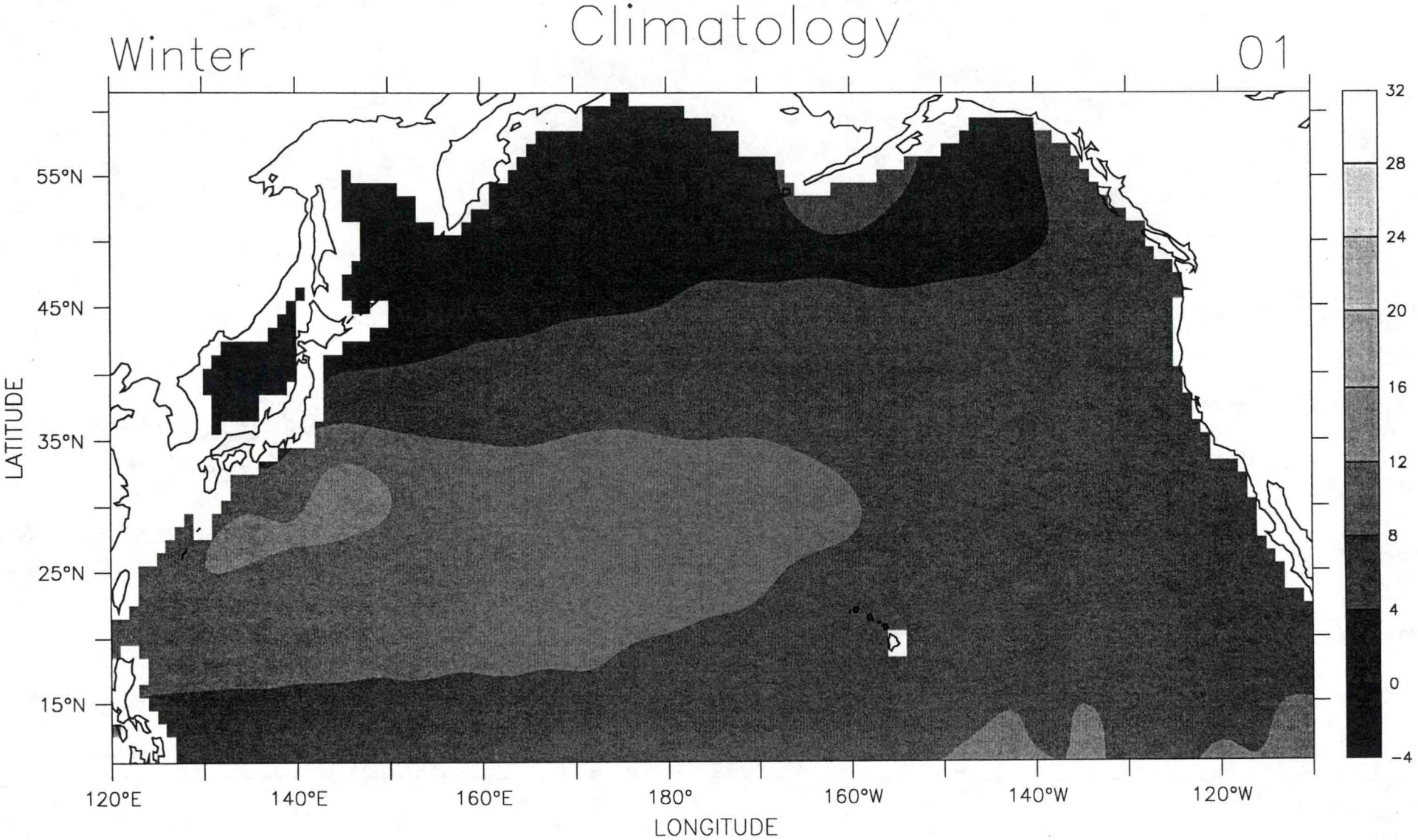

500 m Temperature (C)

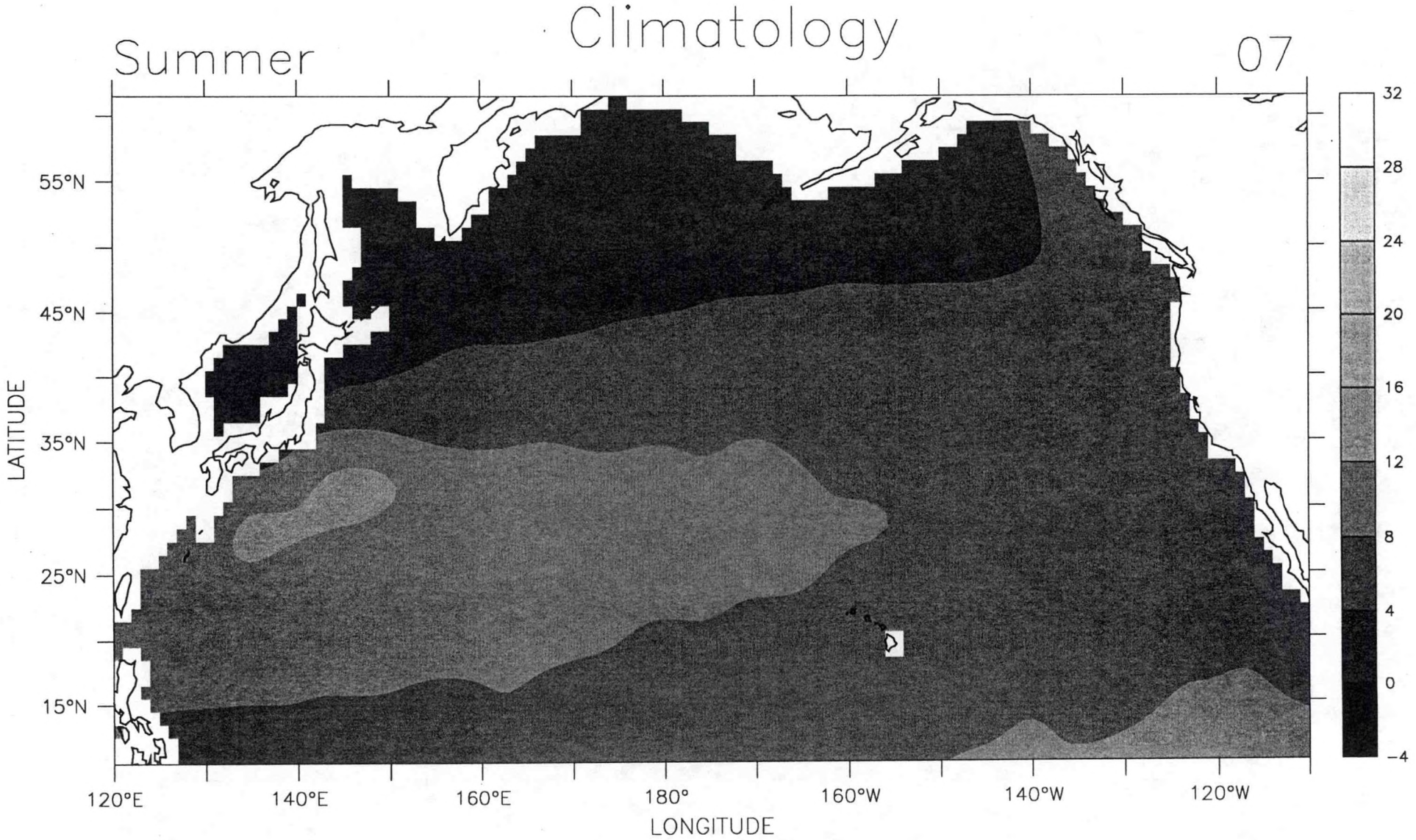

500 m Temperature (C)

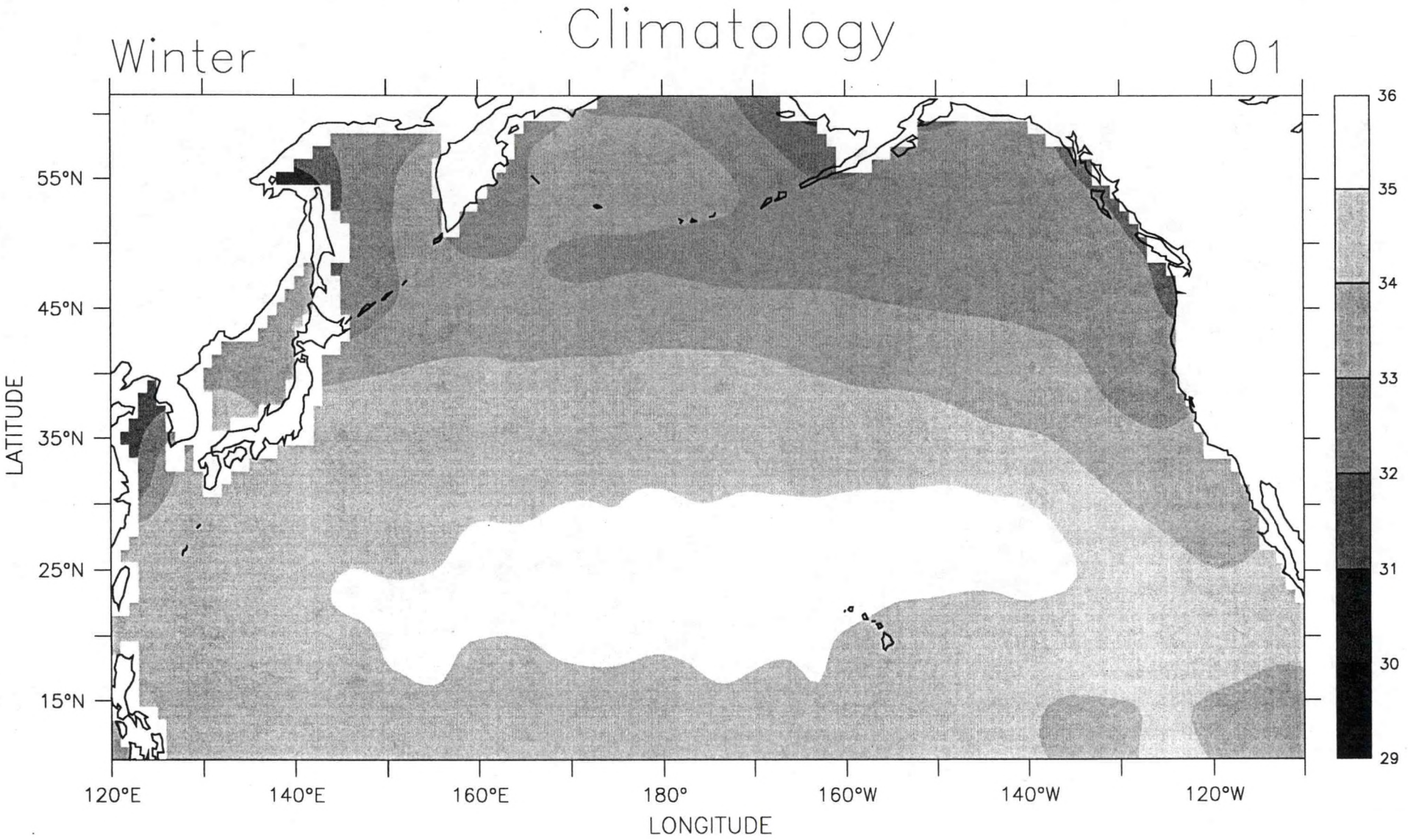

Surface Salinity ($^{o}/_{oo}$)

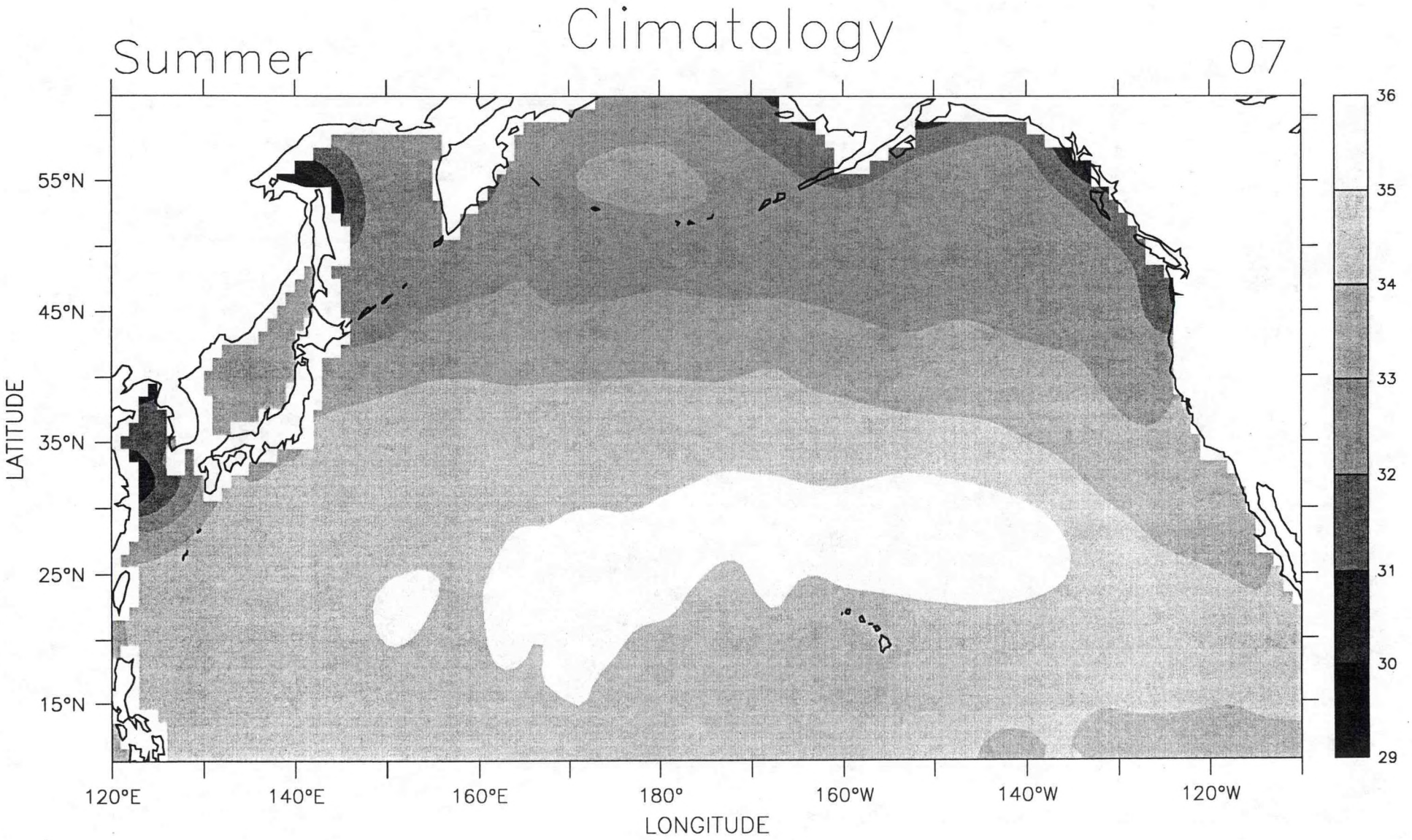

Surface Salinity ($^{o}/_{oo}$)

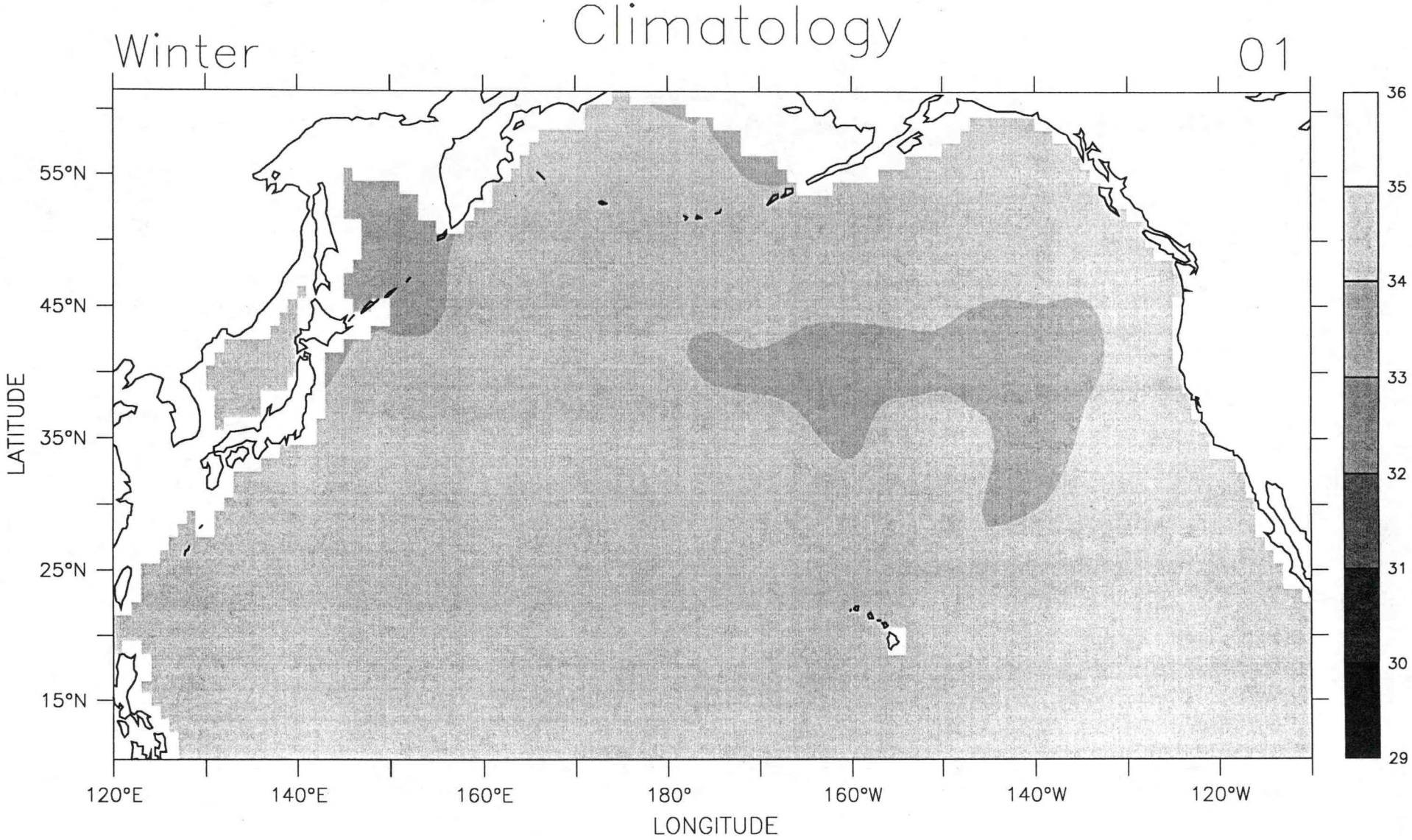

500 m Salinity (°/oo)

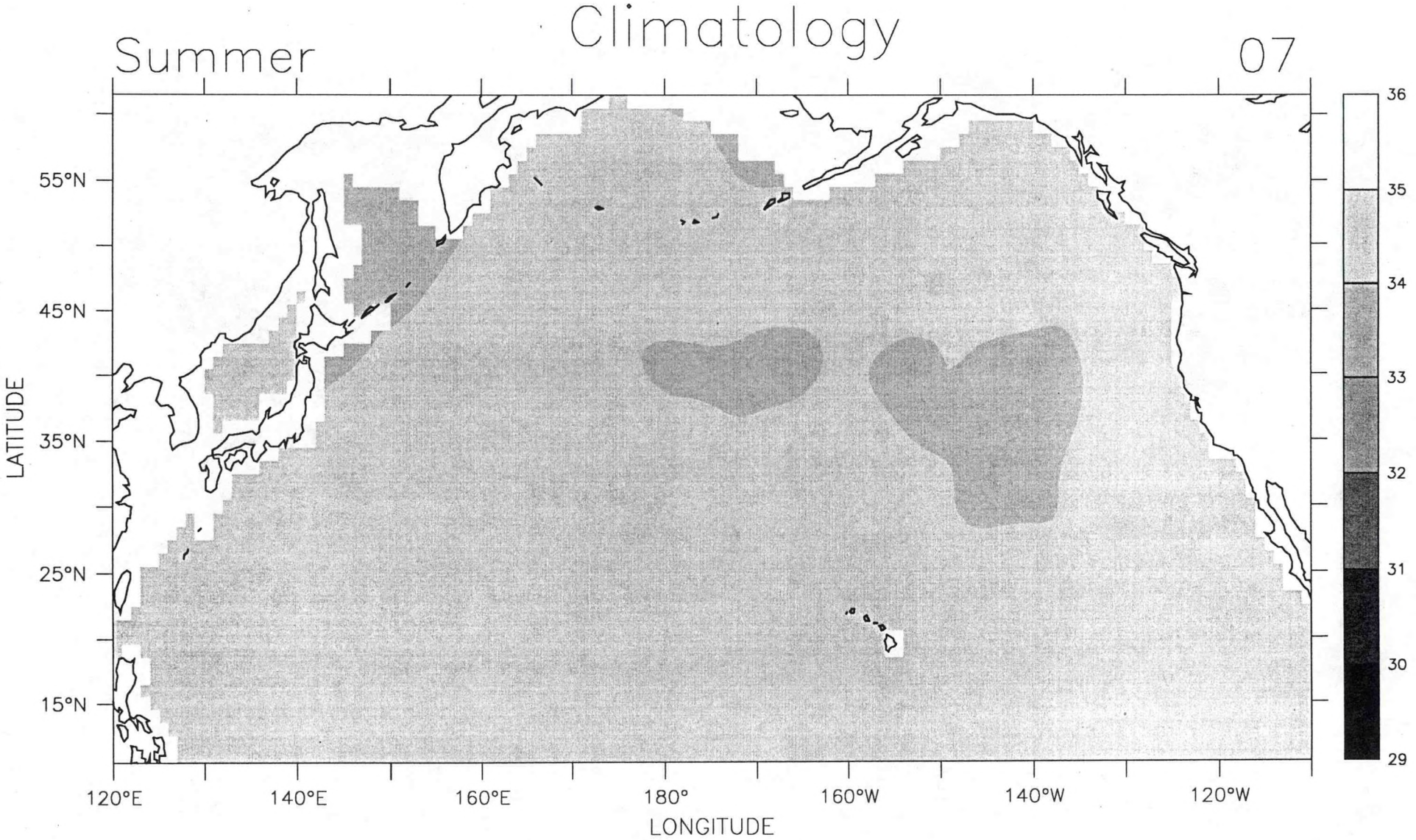

500 m Salinity (°/oo)

1966–1975

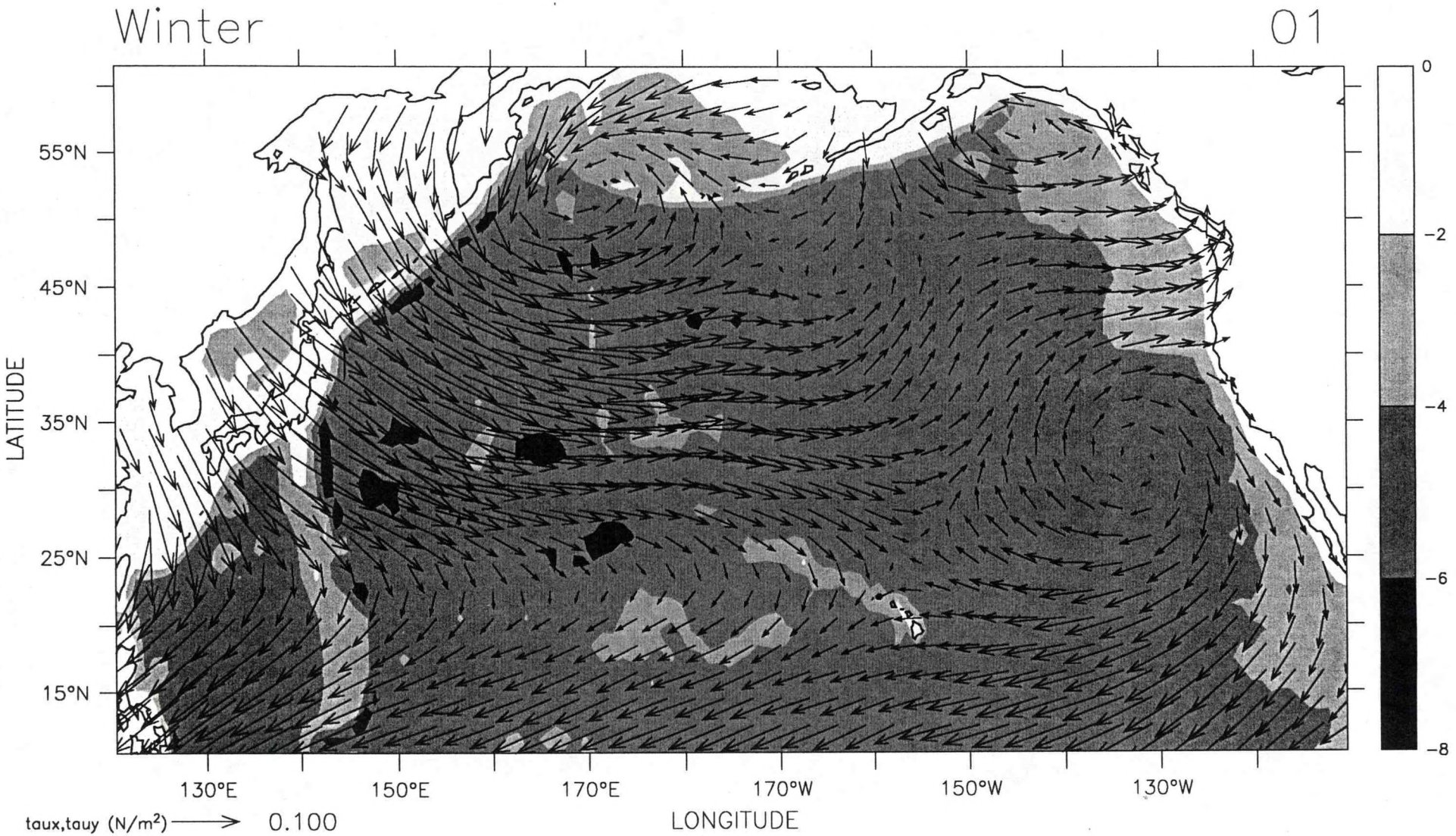

Wind Stress

1966–1975

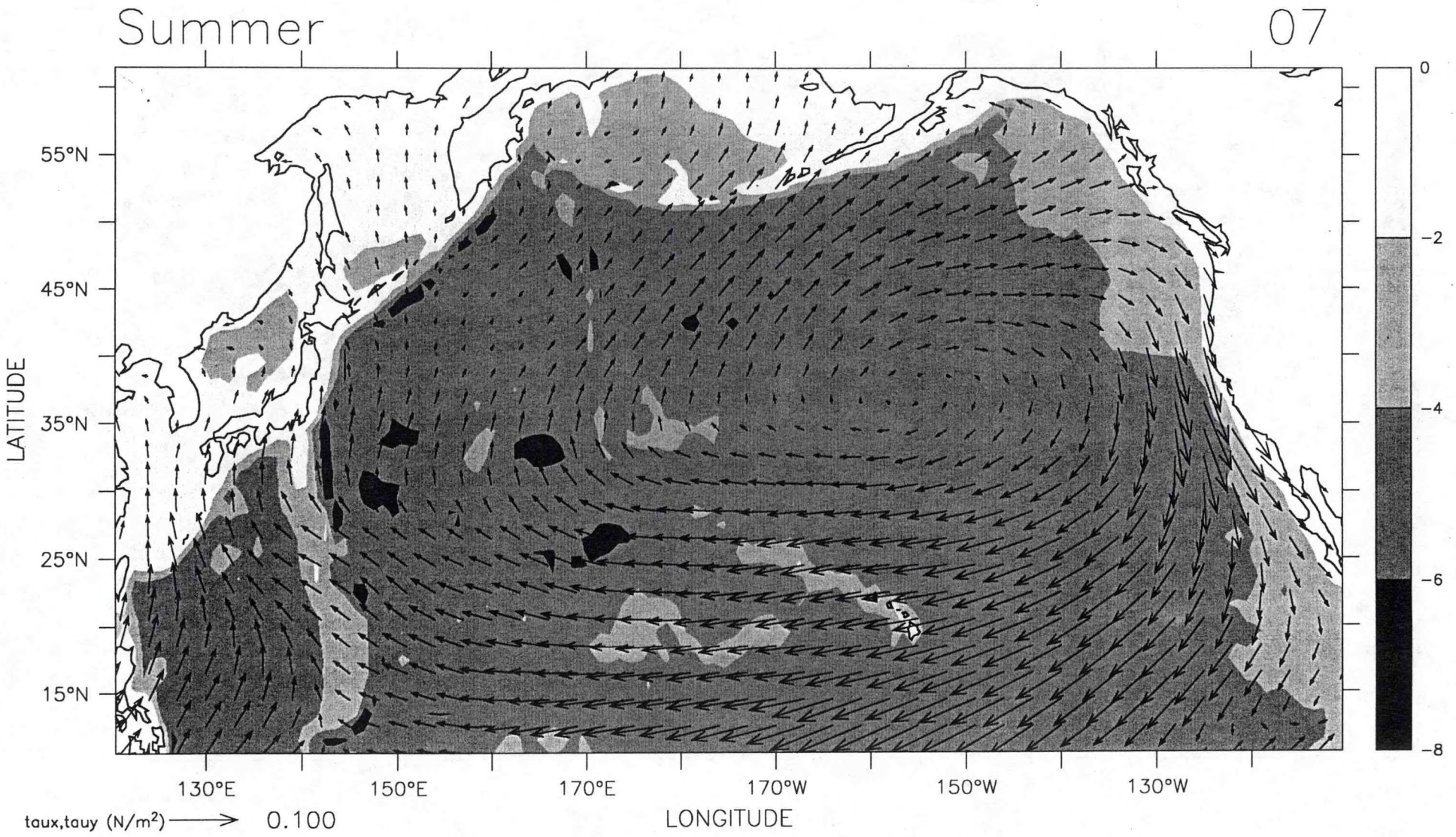

Wind Stress

1977–1986

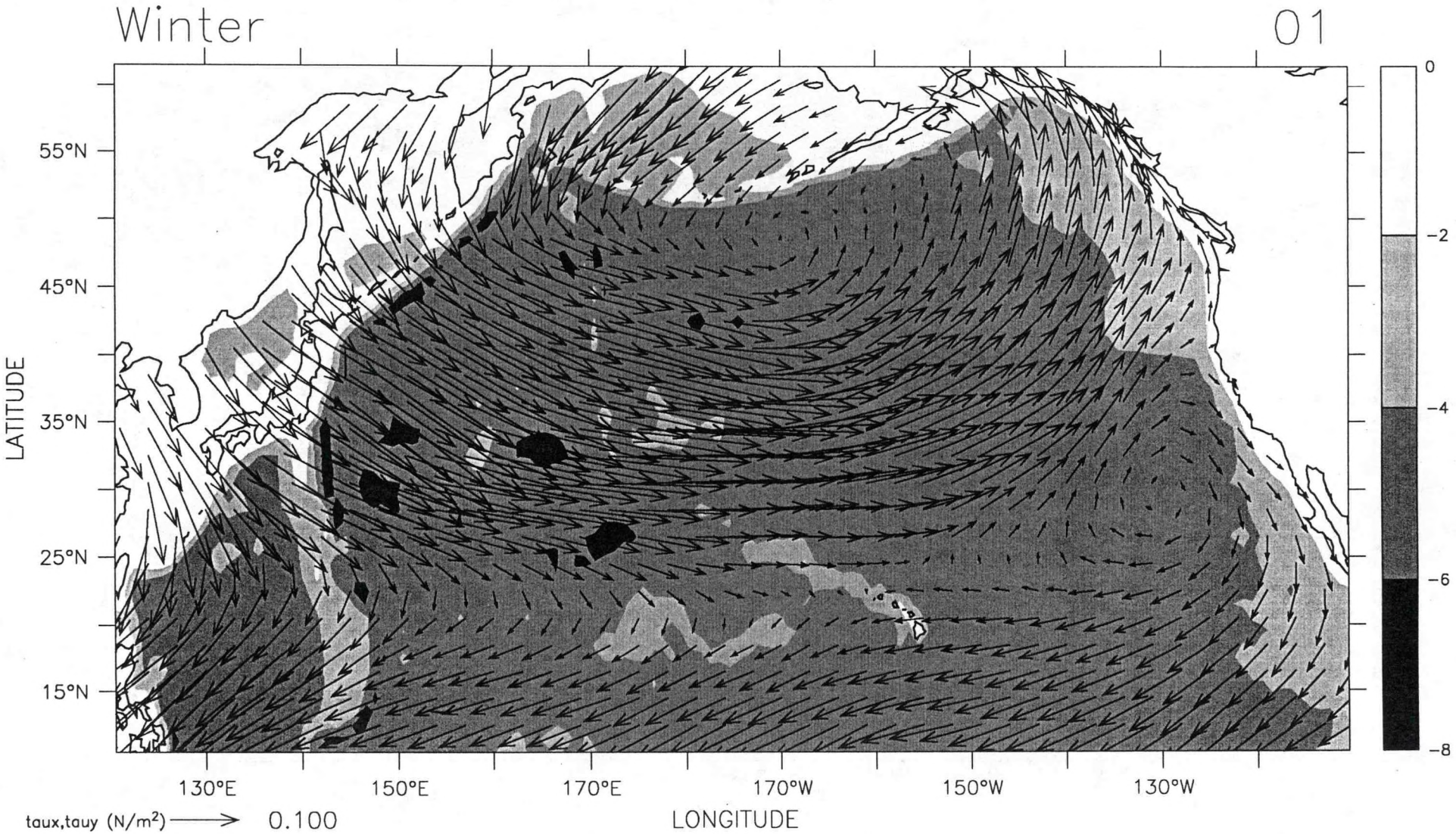

Wind Stress

1977–1986

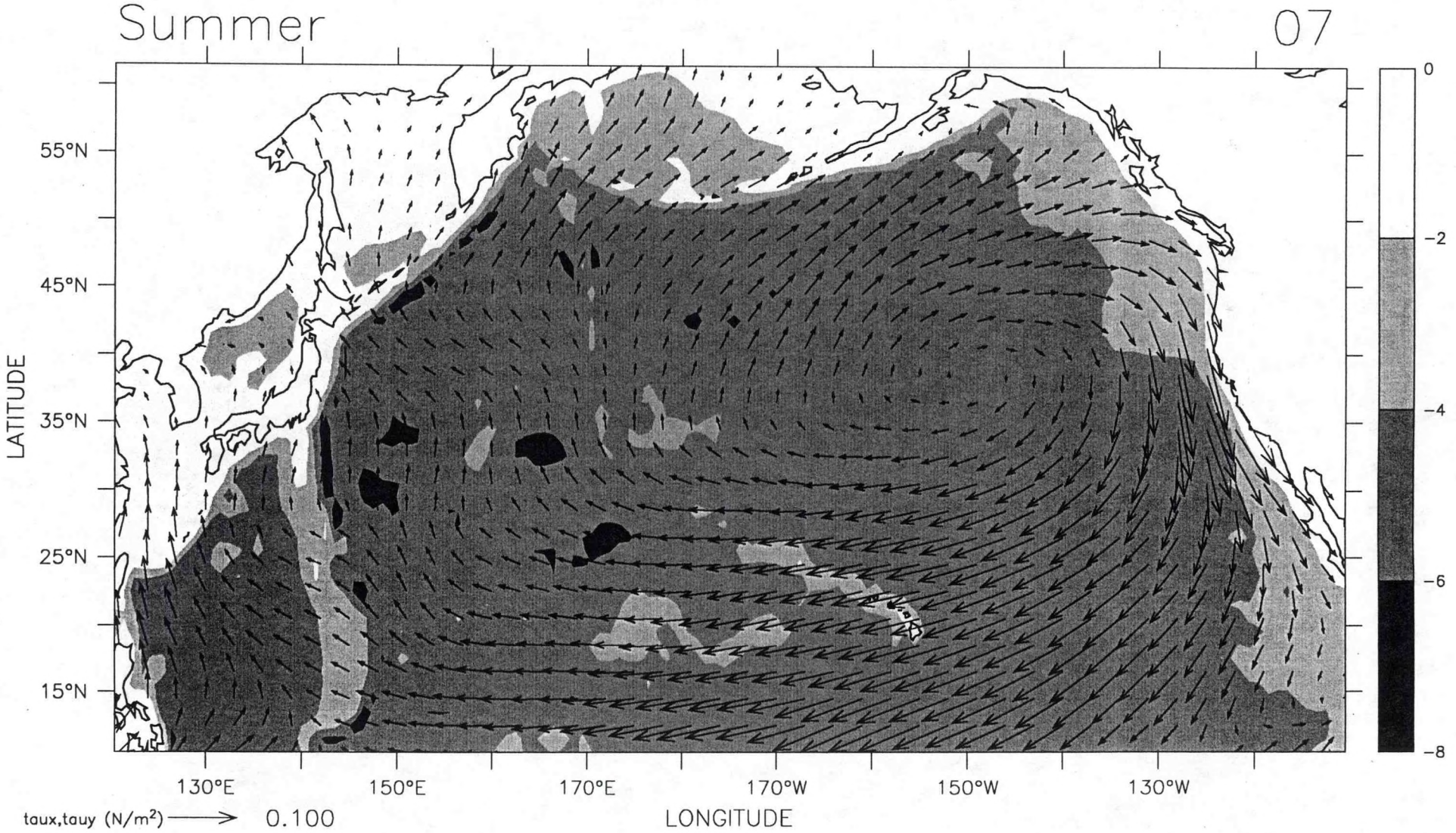

Wind Stress

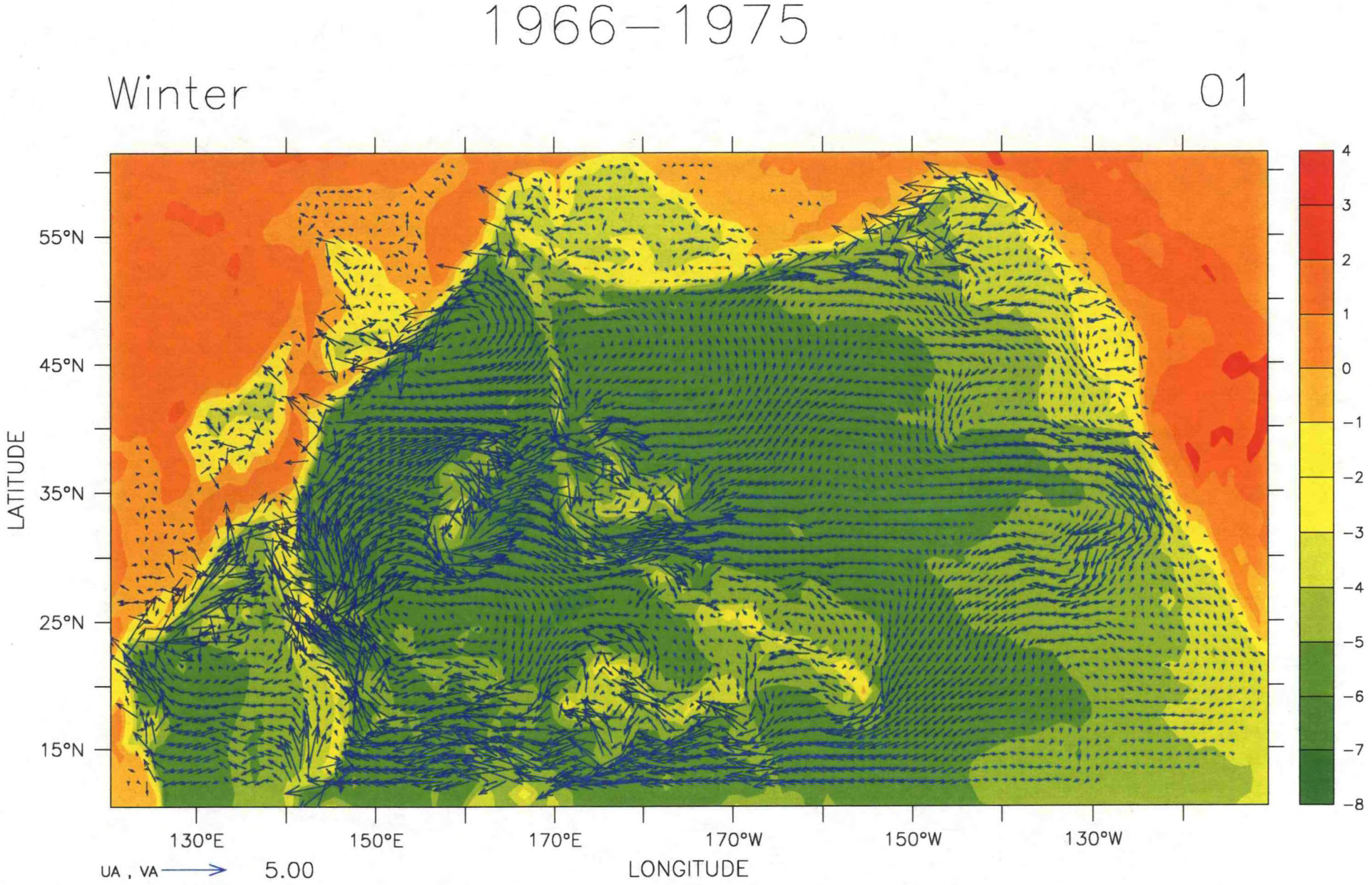

Barotropic plus Ekman transport (Sv)

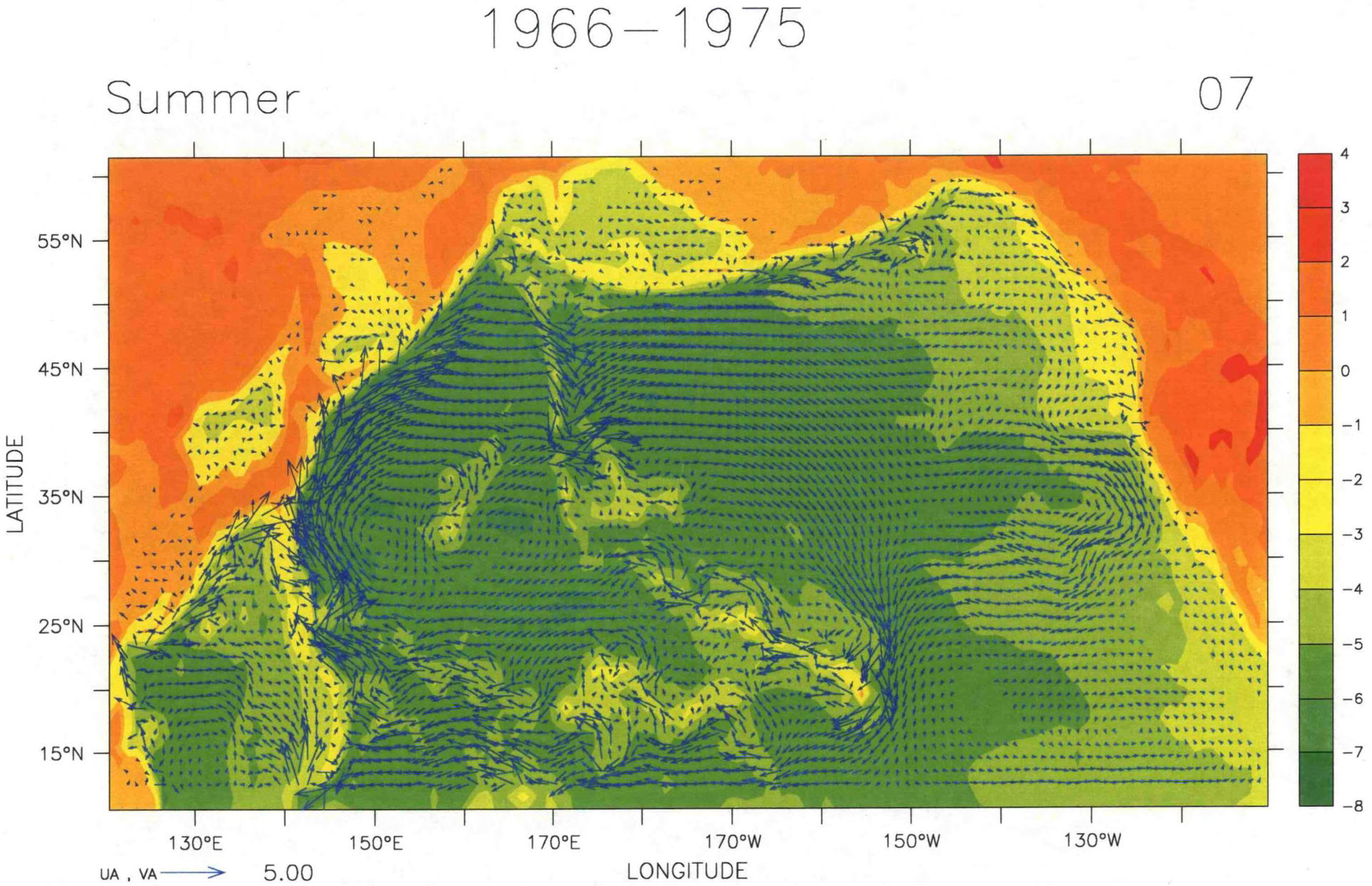

Barotropic plus Ekman transport (Sv)

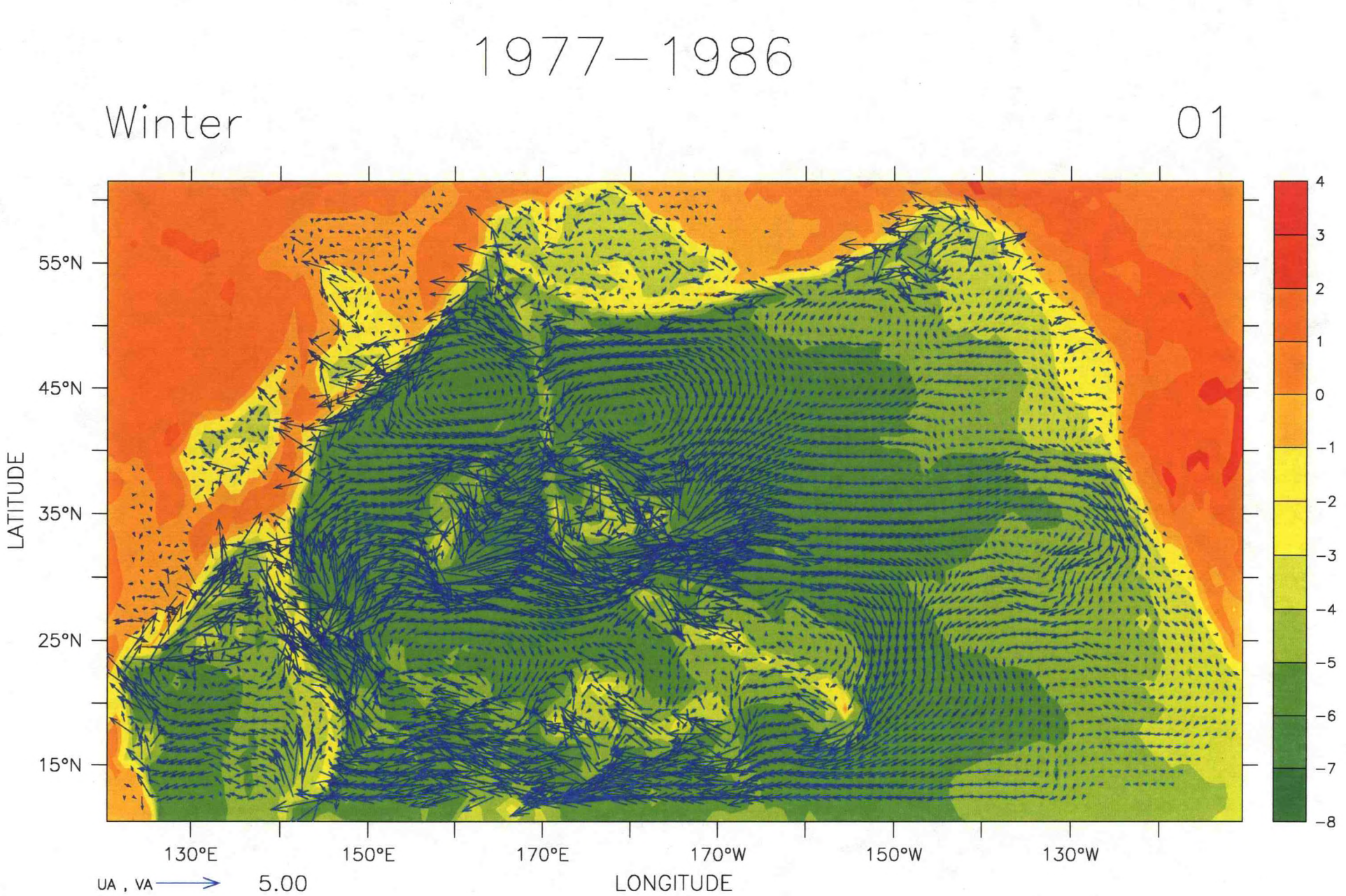

Barotropic plus Ekman transport (Sv)

1977–1986

Summer 07

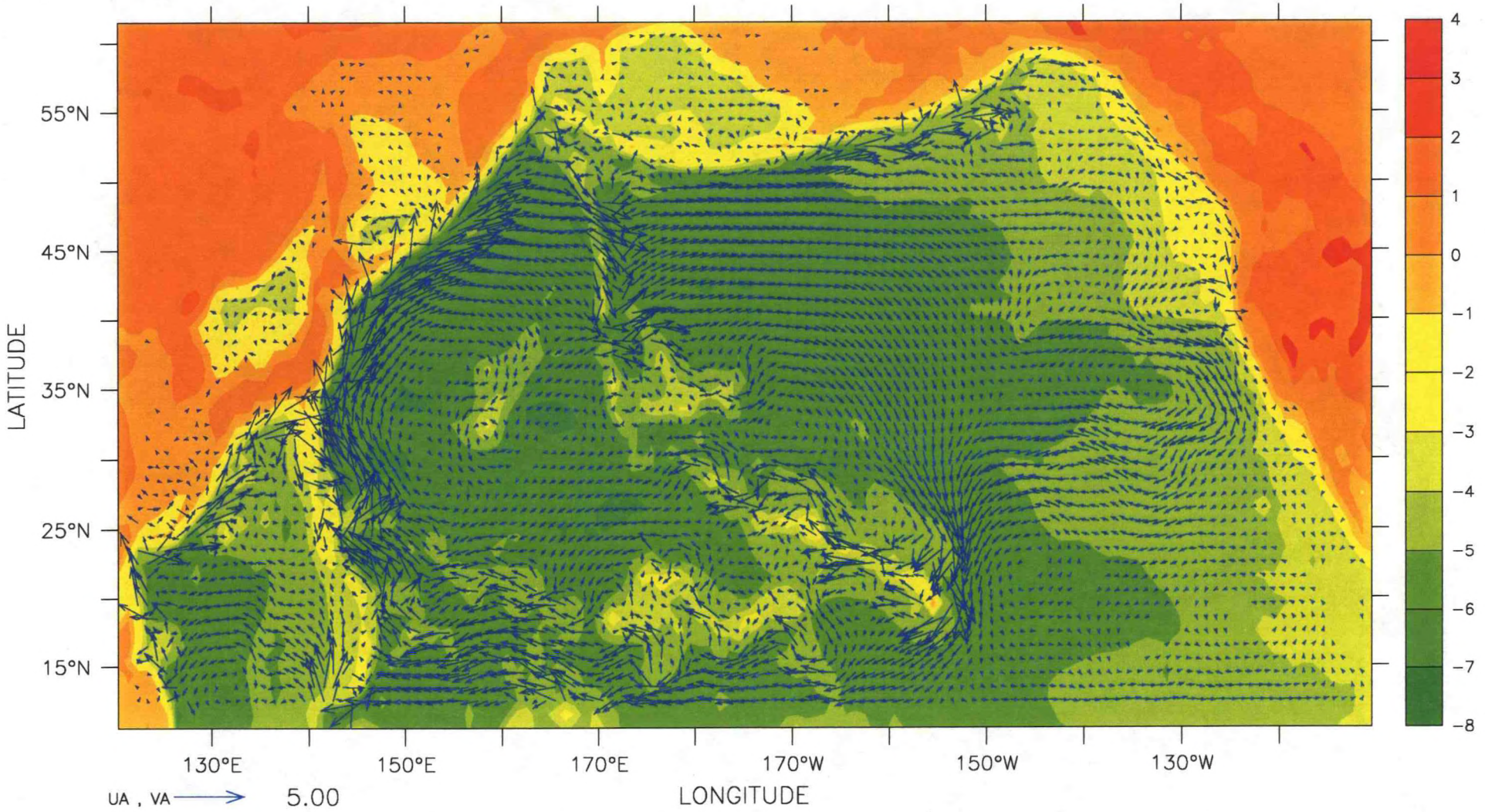

Barotropic plus Ekman transport (Sv)